Laser-Induced Incandescence and Complementary Diagnostics for Flame Soot Characterization

Olofsson, Nils-Erik

2014

Total number of authors:
1

Laser-Induced Incandescence and Complementary Diagnostics for Flame Soot Characterization

Nils-Erik Olofsson

LUND
UNIVERSITY

DOCTORAL DISSERTATION

by due permission of the Faculty of Engineering, Lund University, Sweden.

To be defended at Rydbergsalen, Fysicum, Professorsgatan 1, 23rd January 2015 at 9:15.

Faculty opponent

Dr. Klaus-Peter Geigle, German Aerospace Center, Institute of Combustion Technology, Stuttgart, Germany

Organization LUND UNIVERSITY	Document name Doctoral Dissertation
	Date of issue December 19, 2014
Division of Combustion Physics Department of Physics P.O. Box 118, SE-221 00 Lund, Sweden	CODEN LUTFD2/TFCP-178-SE
Author(s): Nils-Erik Olofsson	Sponsoring organization

Title and subtitle: Laser-Induced Incandescence and Complementary Diagnostics for Flame Soot Characterization

Abstract

This work has been aimed at developing and applying laser-induced incandescence (LII) for flame soot characterization. The basic principle of LII is rapid heating of the soot particles to temperatures of 3500-4000 K by short laser pulses. Thereby the intensity of the soot incandescence is increased. By detection of this increased incandescence and analysis of the detected signal, the volume fraction, particle size and optical properties of the soot can be evaluated. Additionally, both optical and probing techniques have been utilized in combination with LII for studies of specific soot properties.

LII has been applied for characterization of different laboratory flames of interest for soot studies. The soot distribution in flat premixed ethylene/air flames on McKenna burners was found to deviate somewhat from the predicted one-dimensional behavior, where no variation is supposed to be seen radially. A variation was also seen depending on the choice of co-flow gas. Additionally, partially premixed flames burning vaporized n-heptane and n-decane and diluted flat unstrained CH4/O2 diffusion flames were characterized in terms of soot volume fraction distributions.

As the ageing process of soot particles can be followed as height above burner (HAB) in flat premixed flames, these have been utilized as measurement targets for studies of soot formation. Significant differences have been found between newly formed nascent soot and more mature soot. The LII signal response of newly nucleated nascent soot particles in low-sooting flames was found to deviate from what is commonly seen. Instead of displaying an S-shaped fluence curve (signal vs. laser energy) the fluence curve of the nascent soot showed an almost linear trend. Even though these results are challenging to interpret, they show potential for LII as a diagnostic technique for investigations of these newly nucleated soot particles. Evaluation of the absorption function, E(m), showed a significant increase with soot maturity, approaching a nearly constant value of ~0.35 for mature soot. A similar trend was found when combining LII and elastic light scattering for measuring the sublimation threshold i.e. the onset of sublimation. The evaluated sublimation threshold temperature was found to increase with maturity and reach an essentially constant temperature at ~3400 K for mature soot.

When studying processes affecting the decay time of time-resolved LII signals, an increasing level of aggregation of the soot particles was found to increase the decay time. A plausible explanation is an aggregate shielding effect, effectively decreasing the heat conduction rate of the soot. Additionally, by combination of LII and rotational coherent anti-Stokes Raman spectroscopy, a local gas heating effect could be measured. The gas temperature was found to increase ~100 K in a flame with 4 ppm of soot when heating the soot by ~2000 K, effectively increasing the decay time of the LII signal. If not accounting for effects increasing the decay time of LII signals in e.g. soot particle size evaluations, this will lead to an over prediction of the sizes.

Key words: Soot, laser-induced incandescence, combustion, laser diagnostics, combustion diagnostics

Classification system and/or index terms (if any)

Supplementary bibliographical information	Language English

ISSN and key title 1102-8718	ISBN 978-91-7623-205-7

Recipient's notes	Number of pages 235	Price
	Security classification	

Signature _[signature]_   Date   2014-12-08

Laser-Induced Incandescence and Complementary Diagnostics for Flame Soot Characterization

Nils-Erik Olofsson

LUND
UNIVERSITY

Cover image: Photograph by Henrik Bladh.

Nils-Erik Olofsson
Division of Combustion Physics
Department of Physics
Lund University
P.O. Box 118
SE-221 00 Lund, Sweden

Contents

Abstract

This work has been aimed at developing and applying laser-induced incandescence (LII) for flame soot characterization. The basic principle of LII is rapid heating of the soot particles to temperatures of 3500-4000 K by short laser pulses. Thereby the intensity of the soot incandescence is increased. By detection of this increased incandescence and analysis of the detected signal, the volume fraction, particle size and optical properties of the soot can be evaluated. Additionally, both optical and probing techniques have been utilized in combination with LII for studies of specific soot properties.

LII has been applied for characterization of different laboratory flames of interest for soot studies. The soot distribution in flat premixed ethylene/air flames on McKenna burners was found to deviate somewhat from the predicted one-dimensional behavior, where no variation is supposed to be seen radially. A variation was also seen depending on the choice of co-flow gas. Additionally, partially premixed flames burning vaporized n-heptane and n-decane and diluted flat unstrained CH_4/O_2 diffusion flames were characterized in terms of soot volume fraction distributions.

As the ageing process of soot particles can be followed as height above burner (HAB) in flat premixed flames, these have been utilized as measurement targets for studies of soot formation. Significant differences have been found between newly formed nascent soot and more mature soot. The LII signal response of newly nucleated nascent soot particles in low-sooting flames was found to deviate from what is commonly seen. Instead of displaying an S-shaped fluence curve (signal vs. laser energy) the fluence curve of the nascent soot showed an almost linear trend. Even though these results are challenging to interpret, they show potential for LII as a diagnostic technique for investigations of these newly nucleated soot particles. Evaluation of the absorption function, $E(m)$, showed a significant increase with soot maturity, approaching a nearly constant value of ~0.35 for mature soot. A similar trend was found when combining LII and elastic light scattering for measuring the sublimation threshold i.e. the onset of sublimation. The evaluated sublimation threshold temperature was found to increase with maturity and reach an essentially constant temperature at ~3400 K for mature soot.

When studying processes affecting the decay time of time-resolved LII signals, an increasing level of aggregation of the soot particles was found to increase the decay time. A plausible explanation is an aggregate shielding effect, effectively decreasing the

heat conduction rate of the soot. Additionally, by combination of LII and rotational coherent anti-Stokes Raman spectroscopy, a local gas heating effect could be measured. The gas temperature was found to increase ~100 K in a flame with 4 ppm of soot when heating the soot by ~2000 K, effectively increasing the decay time of the LII signal. If not accounting for effects increasing the decay time of LII signals in e.g. soot particle size evaluations, this will lead to an over prediction of the sizes.

Populärvetenskaplig sammanfattning

Även om vi i dagens samhälle försöker minska vårt beroende av förbränningsprocesser är förbränning fortfarande vår största energikälla och förväntas så förbli under en lång tid. Därför är det viktigt att effektivisera förbränningsprocesserna för att maximera den energi som utvinns medan utsläppen samtidigt minimeras. En av de oönskade biprodukterna vid förbränning är sotpartiklar, vilkas effekt på vår omgivning idag är omdiskuterad. Den totala effekten av sotpartiklarna på klimatet är svår att avgöra då sotpartiklar kan verka både värmande och avkylande genom att antingen absorbera eller sprida ljus. Dessutom har sotpartiklar en negativ effekt på vår hälsa. För att öka kunskapen om sot och dess effekter krävs noggrannare mättekniker, inte bara för att avgöra sotets inverkan på klimat och hälsa, utan även för att studera dess bildning och därigenom få ökad kunskap för att minimera utsläppen. Arbetet i denna avhandling har i huvudsak handlat om att utveckla laserbaserade mättekniker för att mäta sotpartiklarnas koncentration, storlek, struktur samt optiska egenskaper. Den teknik som framförallt arbetats med är laserinducerad inkandescens (LII).

Vad är då en sotpartikel? Sotpartiklar bildas i flammor vid ofullständig förbränning, t.ex. i ett stearinljus, en brasa eller en motor. Den gula färgen hos eld är nämligen strålning från varma sotpartiklar i flamman, med en temperatur omkring 1500-2000 °C. Partiklarna är väldigt små, sällan större än en miljondels meter, en hundradel av tjockleken på ett hårstrå och består till största del av kol. Sotpartiklarna förekommer som små runda partiklar, så kallade primärpartiklar. Primärpartiklarna uppträder aningen som separata sotpartiklar eller ihopklumpade i olika formationer som aggregerade sotpartiklar.

Vid en LII mätning hettas sotpartiklarna upp till över 3000 °C m.h.a. intensiva laserpulser. När temperaturen ökar, ökar även intensiteten av strålningen från sotet. Genom att mäta strålningens intensitet kan koncentrationen av sotpartiklar bestämmas och genom att mäta hur signalen från de upphettade sotpartiklarna avtar i takt med att temperaturen minskar, kan man bestämma storleken på partiklarna. Ytterligare analys kan även ge information om sotets optiska egenskaper.

För att generera sot under kontrollerade former används laboratoriebrännare som producerar flammor där förbränningen kan kontrolleras av användaren. I detta arbete har denna typ av flammor uteslutande använts. Därmed har t.ex. studier kunnat göras av hur sotets egenskaper ändras under dess bildningsprocess som kan följas med höjd över brännaren i s.k. flata förblandade flammor. Till de attribut som studerats hör

sotets optiska egenskaper, d.v.s. hur sotet interagerar med ljus. Mätresultaten visar signifikanta skillnader hos de optiska egenskaperna på olika höjder i dessa flammor, d.v.s. sotets optiska egenskaper ändras under bildningsprocessen. Även sotpartikelstorlekar och koncentrationer har uppmätts för att karaktärisera andra laboratorieflammor, data som kan användas för att verifiera förbränningsmodellerares simuleringar. Dessutom har studier gjorts av olika processer som kan påverka utvärderingen av sotpartikelstorlekar. Till exempel har en effekt påvisats som gör att ju mer aggregerad en sotpartikel är, desto långsammare avtar temperaturen efter att de upphettats av en laserpuls. Inkluderas inte detta i utvärderingen kommer storleken överskattas.

Beroende på forskningsfält finns olika intresse för de uppmätta sotegenskaperna. För till exempel motortillverkare är mättekniker med vilka man noggrant kan bestämma partikelkoncentrationer och storlekar betydelsefulla. Detta då det kontinuerligt kommer skärpta restriktioner av partikelutsläppen. För klimatmodellerare är även utvärderade värden av sotets optiska egenskaper viktiga för att de ska kunna förutsäga sotpartiklarnas effekt på klimatet.

List of papers

I. H. Bladh, J. Johnsson, N.-E. Olofsson, A. Bohlin, and P.-E. Bengtsson, *Optical soot characterization using two-color laser-induced incandescence (2C-LII) in the soot growth region of a premixed flat flame.* Proceedings of the Combustion Institute, 2011. 33: p. 641-648.

II. H. Bladh, J. Johnsson, J. Rissler, H. Abdulhamid, N.-E. Olofsson, M. Sanati, J. Pagels, and P.-E. Bengtsson, *Influence of soot particle aggregation on time-resolved laser-induced incandescence signals.* Applied Physics B, 2011. 104(2): p. 331-341.

III. N.-E. Olofsson, H. Bladh, A. Bohlin, J. Johnsson, and P.-E. Bengtsson, *Are Sooting Premixed Porous-Plug Burner Flames One-Dimensional? A Laser-Based Experimental Investigation.* Combustion Science and Technology, 2013. 185(2): p. 293-309.

IV. M.H. de Andrade Oliveira, N.-E. Olofsson, J. Johnsson, H. Bladh, A. Lantz, B. Li, Z.S. Li, M. Aldén, P.-E. Bengtsson, C.C.M. Luijten, and L.P.H. de Goey, *Soot, PAH and OH measurements in vaporized liquid fuel flames.* Fuel, 2013. 112(0): p. 145-152.

V. N.-E. Olofsson, J. Johnsson, H. Bladh, and P.-E. Bengtsson, *Soot sublimation studies in a premixed flat flame using laser-induced incandescence (LII) and elastic light scattering (ELS).* Applied Physics B, 2013. 112(3): p. 333-342.

VI. H. Bladh, N.-E. Olofsson, T. Mouton, J. Simonsson, X. Mercier, A. Faccinetto, P.-E. Bengtsson, and P. Desgroux, *Probing the smallest soot particles in low-sooting premixed flames using laser-induced incandescence.* Proceedings of the Combustion Institute, 2014. 35

VII. E. Nordström, N.-E. Olofsson, J. Simonsson, J. Johnsson, H. Bladh, and P.-E. Bengtsson, *Local gas heating in sooting flames by heat transfer from laser-heated particles investigated using rotational CARS and LII.* Proceedings of the Combustion Institute, 2014. 35

VIII. E. Robert, N.-E. Olofsson, H. Bladh, J. Johnsson, and P.-E. Bengtsson, *Soot formation in unstrained diffusion flames.* Combustion Science and Technology, 2014, DOI: 10.1080/00102202.2014.958219

IX.   N.-E. Olofsson, J. Simonsson, S. Török, H. Bladh, and P.-E. Bengtsson, *Evolution of properties for aging soot in premixed flat flames studied by laser-induced incandescence and elastic light scattering.* Submitted to Applied Physics B, 2014.

X.   J. Simonsson, N.-E. Olofsson, S. Török, P.-E. Bengtsson, and H. Bladh, *Wavelength dependence of extinction in sooting flat premixed flames in the visible and near infrared regimes.* Submitted to Applied Physics B, 2014.

Related work

I.   J. Johnsson, H. Bladh, N.E. Olofsson, and P.E. Bengtsson, *Influence of soot aggregate structure on particle sizing using laser-induced incandescence: importance of bridging between primary particles.* Applied Physics B, 2013. 112(3): p. 321-332.

1 Introduction

Even though environmental consciousness is steadily increasing in the world today, so is the energy consumption. Although the use of eco-friendly alternatives is increasing, like wind and solar power plants, these are far from enough to accommodate the increasing energy consumption. Thus the world's consumption rate of fossil fuels is also increasing, and it has undergone more than a twofold increase since the 70´s, constituting more than 80% of the world's energy supply today [1]. Counting the energy resources from which energy is extracted by combustion, i.e. adding biofuel and waste to the fossil fuels, these constitute over 90% of the total energy supply. According to predictions combustion will also remain the major source of energy during a foreseeable future [1].

As a result of combustion there will be unwanted emissions of different molecular species and particulate matter. These emissions affect climate, environment and health in negative ways, e.g. by increasing the global temperature [2]. The particulate matter originating from combustion is commonly called soot or black carbon and is a result of incomplete combustion. Soot has some characteristic attributes that are of large importance for the environmental and health impacts; it efficiently absorbs visible light, it is refractory and also insoluble in water. In the atmosphere soot has a heating effect through direct absorption of sun light and by acting as condensation nuclei for cloud formation it has a cooling effect by decreasing the sun light reaching the earth's surface. Another example of soot's climate effects is the deposition of soot on the polar ice caps effectively melting the ice. The various effects of soot on the climate make it hard to predict the net effect. In a recent review by Bond et al. [3] the total direct forcing was estimated to +0.88 W/m^2 i.e. a heating effect, however with an uncertainty of 90%. In addition to climate and environmental effects there are also negative health effects. Due to the small size of soot particles they can follow the inhaled air deep into the lungs and also penetrate into the cells and circulatory system, leading to asthma, lung cancer and cardiovascular diseases [4, 5]. As the soot particles are short lived in the atmosphere, with a lifetime of a few days to weeks [3], a decrease of soot emissions would show an almost immediate effect. This has been recognized by politicians and decision makers who have gathered several governments in an effort to reduce short lived climate pollutants [6]. As a result it is of great interest to acquire more knowledge about soot, its properties and its formation in combustion processes.

With various different combustion processes producing soot there are also inherent differences between properties of the emitted soot. For example the size, morphology and optical properties may differ depending on origin of the soot [7, 8]. These are all important attributes when predicting climate and health effects. However, it is a challenging task to characterize soot and there are numerous diagnostic techniques that have been developed for this purpose. The diagnostics techniques can be divided into two categories, probing techniques and optical techniques. The main difference is that probing techniques require extraction of the soot from the measurement position, effectively perturbing any flow or combustion process taking place at that position, while optical techniques are commonly considered as non-invasive in this context. From this point of view optical techniques are often preferable when studying the soot properties and soot formation in combustion processes e.g. laboratory flames. These flames are commonly used within combustion research since they offer the possibility to control the combustion process and study it under stable and reproducible conditions. This is a feature desirable by both experimentalists and modelers.

This thesis work has mainly been aimed at development of the optical diagnostic technique called laser-induced incandescence (LII), a technique commonly used for soot measurements in different combustion processes [9, 10]. The basic principle of the technique is rapid heating of the soot particles by high energy laser pulses, which results in soot temperatures up to ~4000 K. At this high temperature the soot emits intense electromagnetic radiation, both in the visible and infrared wavelength regions. By detecting the emitted radiation and analyzing the detected signal, attributes like the soot concentration, soot particle size and soot optical properties can be evaluated.

The outline of this thesis is as follows. The second chapter gives a description, in accordance with current knowledge, of what soot particles are, how they are formed and what properties they possess. This is accompanied by a discussion about the uncertainties related to the soot properties. In the third chapter the different diagnostic techniques utilized in this work are described with focus on optical diagnostics, in particular the laser-induced incandescence technique. Chapter four deals with the experimental aspects of the work and contains descriptions of the most crucial equipment and discussions about important experimental considerations. In the fifth chapter the results of the work are presented and interesting aspects and implications are discussed. Finally, the work is summarized in chapter six.

2 Combustion generated soot

Soot consists of small relatively spherical particles in the size range ~5-50 nm or aggregates of these small particles and is mainly composed of carbon and some fraction of hydrogen. Most people probably relate soot to some kind of combustion. However, not all combustion will generate soot particles. There are two prerequisites that must be fulfilled for a combustion process to generate soot. Firstly, the fuel should contain both carbon, C, and hydrogen, H, i.e. some kind of hydrocarbon should be burnt. As an example, combustion of pure hydrogen gas, H_2, will not emit soot particles due to the lack of carbon. Secondly, the combustion of the fuel should be incomplete. Otherwise there will be no fuel fragments from which the soot particles are formed. In this chapter both soot and its formation will be discussed.

2.1 What is soot?

The answer to the question "What is soot?" is a bit complicated since there is no precise definition of what soot really is. What is considered as soot somewhat differs between different research fields. In a review by Bond et al. [7] the current state of terminology concerning carbon and carbonaceous material is discussed in detail. For the sake of simplicity, from now on in this thesis, soot will be considered as combustion-generated carbonaceous particles.

Soot consists mainly of carbon, but there is also significant hydrogen content (~1% by weight [11]). Depending partly on the H/C ratio the soot will have different structure and properties, see section 2.2 and 2.3. The soot particle size is typically very small, in the range 10-100 nm, but there are cases where soot particles have been seen to grow to sizes up to ~100 micrometers, see for example [12] and Paper VIII.

The soot particle size and structure differs depending on the environment i.e. flame conditions. Generally one can say that soot is built up of spherical (or close to spherical) primary particles in the size range ~5-50 nm. These primary particles can either be isolated or grouped together in the form of soot aggregates consisting of 2 or more primary particles. In Figure 2.1 a transmission electron microscopy (TEM) image of soot aggregates is displayed, see section 3.1 for a description of TEM. The structure of these aggregates is commonly described mathematically as a fractal structure [13],

$$N_p = k_f \left(\frac{R_g}{a}\right)^{D_f},\qquad(2.1)$$

where N_p is the number of primary particles in the soot aggregate, k_f is a proportionality constant often denoted as the fractal prefactor, R_g is the radius of gyration (a measure of the aggregate size), a is the primary particle radius and D_f is the fractal dimension. This theoretical description of aggregates is useful since it provides measurable quantities so that soot aggregates can be characterized, and thus modelled and experimentally measured. It should be noted that this theoretical description of fractal aggregates assumes spherical primary particles and point contact between them, and as seen in Figure 2.1 this is a simplification of the reality.
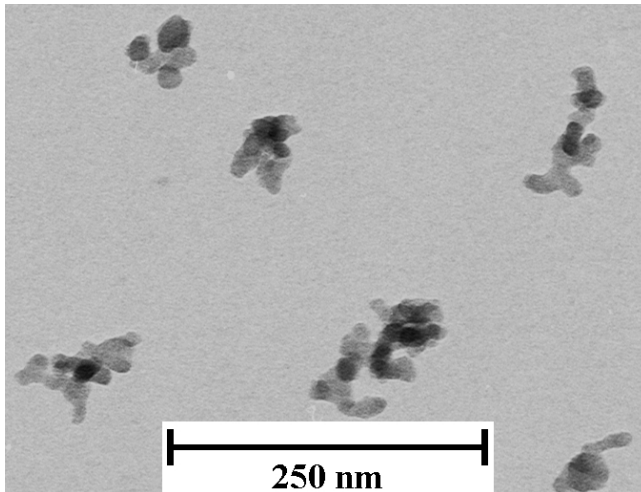
Figure 2.1
A TEM image of aggregated soot particles from a flat premixed ethylene/air flame (see section 4.1.1).

2.2 Soot formation

Soot originates from some kind of combustion process, i.e. an exothermic reaction between two or more reactants. For combustion to take place one of these reactants must be an oxidizer and another must be a fuel. The oxidizer releases chemically bound energy from the fuel by oxidation, which is why a combustion process releases heat, i.e. an exothermic reaction. The most commonly used fuel both in the work presented in this thesis and within the LII community is ethylene (C_2H_4) and the most commonly used oxidizer is air (or more precisely the oxygen, O_2, in air). The combustion of ethylene and air can be described by the following global reaction

$$C_2H_4 + 3O_2 \rightarrow 2H_2O + 2CO_2, \qquad\qquad (2.2)$$
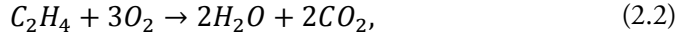
which describes the complete or stoichiometric combustion process, meaning that all fuel and oxidizer is consumed. For hydrocarbon fuels this results in the products water, H_2O, and carbon dioxide CO_2. However, the global reaction does not show any of the intermediate reactions taking place, called elementary reactions. There are numerous elementary reactions before the final products are formed and for a stoichiometric process the intermediately formed products are consumed. On the other hand, if there is excess fuel there will be other products in addition to the water and carbon dioxide. A way of defining the fuel-oxidizer mixture strength is through the equivalence ratio, defined as

$$\phi = \frac{\left(n_{fuel}/n_{oxidizer}\right)_{gas\,mix.}}{\left(n_{fuel}/n_{oxidizer}\right)_{stoich.mix.}}, \qquad\qquad (2.3)$$

where n denotes the number of moles of either fuel or oxidizer. When $\phi = 1$ the combustion process is stoichiometric. For $\phi < 1$ the combustion is called lean, and when $\phi > 1$ it is called rich. Increasing the equivalence ratio above one leads to formation of carbon monoxide, CO, and hydrogen, H_2, in addition to the H_2O and CO_2. Further increasing ϕ will eventually lead to the formation of larger aromatic hydrocarbons and soot particles ($\phi \gtrsim 1.5$, depending on the fuel used).

In Figure 2.2 there is a schematic illustration of the soot formation process, starting from the left in the figure. The start of soot formation is the pyrolysis of fuel i.e. high temperature makes the fuel break down into smaller hydrocarbons. One of the most abundant of these smaller hydrocarbons is acetylene, C_2H_2, which also is one of the most important molecular building blocks for soot particles [8]. The next step in the soot formation process is the formation of aromatic hydrocarbons, which then grow by addition of other aromatics and smaller hydrocarbons to form larger polyaromatic hydrocarbons (PAH). One likely pathway for this PAH growth process is the hydrogen-abstraction-carbon-addition (HACA) mechanism, see [8] and references therein. The PAHs are often denoted as soot precursors, since they are believed to be the origin for nucleation of soot particles. However, the details of the nucleation process are still a subject of research. There are several different potential pathways from PAHs to soot nuclei [8, 14]. The first nucleated soot particles are of sizes around 1 nm [8]. These soot particle nuclei then grow by the addition of smaller hydrocarbon molecules, like acetylene, to the particle surface, a process called surface growth. Additionally, there is coagulation occurring simultaneously with the surface growth. This means that the soot nuclei collide and stick together to form larger soot particles, and is one of the reasons that the soot primary particles are not completely

spherical. Later in the soot formation process the formed soot particles adhere to each other to form soot aggregates, like the ones seen in Figure 2.1. The pathways and precise mechanisms for the steps in the soot formation process are still subject of research, see [8, 14] and references therein for a thorough review of the subject.
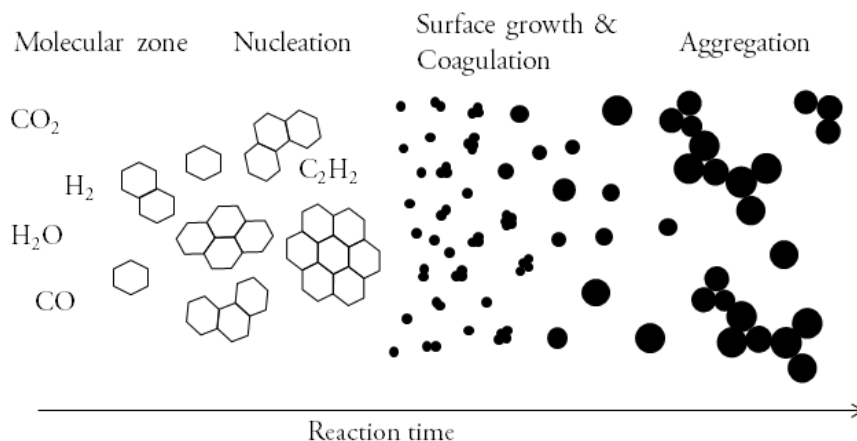

Figure 2.2
A schematic illustration of the soot formation process showing how the growth process starts with molecules and ends with large soot aggregates.

It is not only the size that changes with soot growth, but also the structure of the soot particles. The newly formed soot particles, with sizes of a few nanometers, are referred to as nascent soot particles. These have been shown to exhibit a liquid-like structure [8, 14-18] by studying how they spread onto substrate surfaces using TEM and atomic force microscopy (AFM). As the soot particle surface growth and coagulation cease later in the soot formation, the surface of the soot particles becomes less reactive and also more solid. During the aging of the soot, hydrogen is abstracted and carbon is added to the particles, effectively decreasing the H/C ratio [7, 8, 19-21]. Thus the H/C ratio is sometimes used as a measure of soot age, or maturity. Soot late in the formation process is often denoted as mature i.e. the soot surface reactivity has decreased considerably and the soot properties have stabilized. By high-resolution TEM and X-ray analysis, it has been shown that a graphitization process occurs at the later stages of the soot formation [22-26]. This graphitization results in an onion-like shell-structure of the mature soot particles due to ordered graphitized carbon layers around an amorphous core, see Figure 2.3 for an illustration of a graphitized soot aggregate. The graphitization can be explained by the abstraction of hydrogen leading to a transformation from amorphous carbon to carbon clusters with sp^2 bonds, like the bonds between carbon in graphite [7]. For interested readers there are numerous sources for more information about combustion and soot formation, e.g. [8, 11, 14, 27-29].
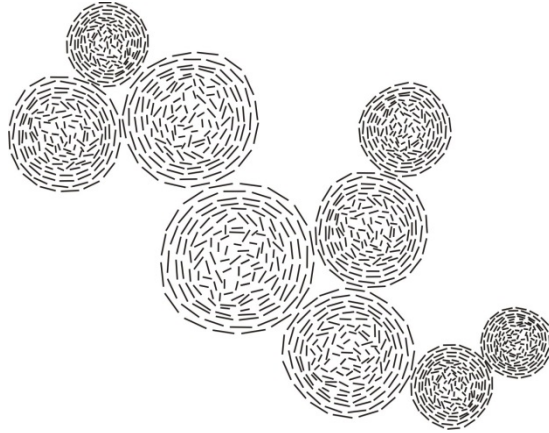
12

Figure 2.3
A schematic illustration of an aggregated and graphitized, mature soot particle with an onion-like
structure. The outer graphitized carbon forms an ordered shell around the amorphous core.

2.3 Soot properties

Knowledge of soot properties is very important to understand and predict the impact soot has on both environment and human health. However, measuring these properties, especially without affecting them at the same time, is very challenging.

Two important physical properties of soot are the density, ρ_s, and specific heat capacity, c_s. Commonly used values for mature soot at flame temperature are ~1.8 g/cm³ for the density [30, 31] and ~2100 J/kgK for the specific heat, which is the value for solid graphite [32]. Suggested temperature dependent expressions for ρ_s and c_s can be found in [32]. However, to add to the complexity, these two properties are likely to differ between mature and nascent soot due to the large structural differences. In [33, 34] the density of nascent soot particles is suggested to be ~1.2 g/cm³, a value significantly lower than the commonly used density for solid graphite. On the other hand, one can argue that a lower density of the nascent soot is reasonable considering the much higher hydrogen content compared to mature soot. Available sources for data on the variation of c_s with maturity are very scarce, but it is not farfetched to assume that there also is a variation of the specific heat. The impact of possible variations of ρ_s and c_s with soot maturity on the work presented in this thesis is discussed in Paper I and V.

The optical properties of soot are central when describing the interaction between light and soot particles, e.g. the absorption, emission and scattering of laser light. When describing the light-soot interaction the complex refractive index, m, of the soot is a crucial property,

$$m = n - ik. \tag{2.4}$$

As will be further explained in section 3.2, the complex refractive index affects the absorption and emission of light by soot through the absorption function,

$$E(m) = -\text{Im}\left(\frac{m^2-1}{m^2+2}\right), \tag{2.5}$$

and the scattering of light through

$$F(m) = \left|\frac{m^2-1}{m^2+2}\right|^2. \tag{2.6}$$

The value of m for soot is inherently challenging to quantify, not only due to limitations of the measurement techniques, but also due to variations with maturity, wavelength and temperature etc. [7, 35]. Paper I, V, IX and X, are examples of studies where the value and wavelength dependence of $E(m)$, or more specifically $E\big(m(\lambda)\big)$, and how the wavelength dependence changes with maturity are discussed.

Soot particles are very efficient absorbers and emitters of electromagnetic radiation, i.e. light, both in the visible and infrared regions. In the visible region this efficiency can be identified by the yellow luminosity of sooting flames and in the infrared it can be identified by the emitted heat. The intensity, or irradiance, of the radiation emitted by a soot particle is close to that of a black body and can thus be described by the Planck radiation law weighted by the emissivity of the soot as,

$$I\big(d_p, \lambda, T\big) = \varepsilon\big(d_p, \lambda\big) \frac{2\pi h c^2}{\lambda^5 \big(\exp\big(\frac{hc}{\lambda k_B T}\big)-1\big)}, \tag{2.7}$$

where d_p is the primary particle diameter, λ is the wavelength of the emitted electromagnetic radiation, T is the soot temperature, h is the Planck constant, c is the speed of light, and k_B is the Boltzmann constant. Assuming that the particle is spherical and fulfills the Rayleigh criterion, $d_p \ll \lambda$, the emissivity can be expressed as

$$\varepsilon\big(d_p,\lambda\big) = \frac{4\pi d_p E(m(\lambda))}{\lambda}. \tag{2.8}$$

When the Planck radiation is scaled down by an emissivity the emitting object is commonly called a gray body. In the case of larger aggregated soot particles, which can violate the Rayleigh criterion, the Rayleigh-Debye-Gans (RDG) theory is often applied. The RDG theory implies that the even though an aggregated particle itself is not within the Rayleigh limit, it may be divided into subunits that fulfill the Rayleigh criterion and assuming they do not interact with each other, Rayleigh theory is applicable [36, 37]. This means that for an aggregated soot particle, the emitted intensity is the expression in (2.7) multiplied by N_p. The error induced by assuming RDG theory for the absorption and emission by aggregated soot particles has been investigated by Liu et al. [38]. A more thorough description of the absorption and emission of light by small particles can for example be found in [37].

3 Soot diagnostics

There are several different ways to detect and characterize soot. The simplest method is to visually study the yellow luminosity of hot soot particles, for example in a flame, since this can be done by the naked eye without any aid of advanced equipment. However, to achieve any quantification, more advanced techniques will be required. These can be divided into probing techniques and optical techniques. The difference between these two categories is that with probing techniques the soot must be extracted from the measurement location by some kind of probe and then analyzed ex situ, while optical techniques use information carried by light and thus the measurement can be made directly at the measurement location, in situ. The work presented in this thesis is focused on optical techniques and thus the main part of this chapter will deal with optical techniques.

3.1 Probing techniques

There are a multitude of different probing techniques for measurements of soot and other small particles. These techniques are frequently used within the aerosol research field. It is however not within the scope of this thesis to describe the variety of probing techniques in detail. Nonetheless, the techniques used for the work in this thesis will briefly be explained. Scanning mobility particle sizing (SMPS) and a differential mobility analyzer (DMA) combined in series with an aerosol particle mass analyzer (APM), DMA-APM for short, were used in Paper II.

An SMPS system is a combination of three different components: a bipolar charger, a DMA and a condensation particle counter (CPC). The bipolar charger is used to achieve a bipolar equilibrium charge distribution of the soot particles [39] needed for the DMA. After passing the bipolar charger the soot enters the DMA which is used to sort out particles of a certain electric mobility diameter, i.e. a diameter related to how a sphere with a certain electric charge would move in air when subject to an electric field [40]. This is achieved by using a flow of air to transport the charged particles through an electric field. Particles with a specific electric mobility diameter will exit through an exit slit, while all other particles will follow the air flow to an exhaust. By varying the strength of the electric field, the electric mobility diameter of the particles exiting through the slit can be chosen. The number of exiting particles per size

interval is then counted by a CPC and thus an electric mobility diameter distribution is achieved i.e. a size distribution of the soot particles.

In the DMA-APM an APM [41] is used to determine the mass of the particles exiting the DMA. The APM consists of two concentric cylindrical electrodes rotating at the same angular speed and by applying a voltage an electric field is created between the electrodes. When the charged particles exiting the DMA are introduced at one end between the two electrodes only the particles subject to an electric force equal to the centrifugal force will exit at the other end. By variation of the angular speed and applied voltage the mass of the particles passing the APM can be controlled. The number of passing particles is then counted by a CPC, resulting in a mass distribution of the particles. Those interested in more information about aerosol science and probing techniques are referred to [39] and references therein.

Microscopy techniques can also be listed under the probing techniques category. Among these, transmission electron microscopy (TEM) is a commonly used method for soot particle studies, making it possible to evaluate the size and structure of the particles [15, 22, 39, 42-44]. TEM has also been used for characterization of soot particles in Papers I, II and VIII. The principle of TEM can be compared to that of a conventional optical microscope, but a beam of electrons is used instead of light. This requires that the inside of the microscope is under a high vacuum (<0.01 Pa). Thus TEM is limited to studies of solid matter that does not evaporate or degrade under the low pressure and heating by the electron beam. The electron beam is controlled by magnetic lenses and soot particles subject to the electron beam will scatter and absorb electrons. This can be used to achieve a two-dimensional silhouette image of the soot, which can then be utilized for characterization of soot primary particles and aggregates.

For insertion of the soot particles into the electron microscope they must first be extracted from the flame and deposited on a small grid covered by a thin carbon film. For this there are different techniques, but when working with flames a commonly used technique is to quickly insert and extract the grid at the measurement location in the flame e.g. by a pneumatic probe. Since the grid is much colder than the flame the soot particles will stick to the carbon film due to a thermophoretic force arising from the steep temperature gradient. Thus this technique of collecting soot particles is called thermophoretic sampling.

In addition to TEM, also atomic force microscopy (AFM) and scanning electron microscopy (SEM) are used for soot studies [12, 17, 18, 45, 46].

3.2 Optical techniques

Optical techniques always require a light source of some kind since it is the light that carries the information. This light source can for example be a lamp, a flame, the sun or a laser. The light source can be used in very different ways for measurements. For example, the emitted light can be measured directly to characterize the emitting source, it can also be used to induce a light signal from some other source e.g. a molecule or a particle and it can also be transmitted through a medium to study absorption phenomena etc. There is one inherent advantage with all optical diagnostic techniques. The measurement is done remotely without need of a probe at the measurement location, making it possible to measure in very harsh environments, e.g. high temperatures, without inducing perturbations at the measurement location. However, with this follows a limitation as well since optical access is required to collect and measure the light.

In this work the optical techniques used are all based on the use of laser as light source. The laser gives some additional advantages to the already mentioned one. Due to the high intensity of the laser light it can be used to induce signals that cannot be achieved with other light sources. The measurements can be done as point measurements, where the laser light is focused to a small measurement point, or along a line as a line of sight measurement. The laser light can also be shaped to a sheet, making 2D measurements possible and with the high repetition rate lasers that are available today it is possible to do 3D measurements by rapidly scanning a 2D sheet over a volume [47] and even time-resolved 3D measurements have been made [48]. Additional, commonly mentioned benefits are the high temporal and spatial resolutions achievable.

3.2.1   Laser extinction

Laser extinction is a commonly used line of sight technique for characterization of soot particles, especially in combination with other laser diagnostic techniques [49-55]. On its own, laser extinction is regularly applied for measurements of soot volume fractions of soot particles dispensed in some medium (usually a gas, e.g. in a flame) [56, 57]. Assuming spherical and monodisperse primary particles with diameter d_p, the soot volume fraction can be defined as

$$f_v = N \frac{\pi d_p^3}{6},$$

(3.1)

with N denoting the particle number concentration in the medium. One of the reasons that laser extinction is so commonly applied is that it is a simple technique

19

and it does not require a lot of expensive apparatus, as opposed to more advanced laser diagnostic techniques. Hence it is also fast to set up and does not require much space.

The laser extinction technique is based on the phenomenon that light propagating through a volume of medium with dispensed particles will get attenuated due to absorption and/or scattering in the wavelength region of the incident light. Thus the transmitted light will have a lower intensity than the incident light, schematically illustrated by Figure 3.1. This attenuation, or extinction, of light can be described by the Beer-Lambert law,

$$I_T = I_0 \exp(-\sigma_{ext} L N), \tag{3.2}$$

where I_T denotes the irradiance of the transmitted light, I_0 the irradiance of the incident light, σ_{ext} the average extinction cross-section of the dispensed particles and L is the path length through the volume of dispensed particles. For the Beer-Lambert law to hold, the particles must be homogenously distributed in the medium and spaced so that they do not interact by e.g. multiple scattering. The extinction consists of two parts, absorption and scattering, and thus the extinction cross-section is the sum of the absorption cross-section, σ_{abs}, and the scattering cross-section, σ_{scat},

$$\sigma_{ext} = \sigma_{abs} + \sigma_{scat}. \tag{3.3}$$

The extinction coefficient can then be defined as,

$$K_{ext} = N\sigma_{ext} = K_{abs} + K_{scat}, \tag{3.4}$$

where K_{abs} is the absorption coefficient and K_{scat} is the scattering coefficient.
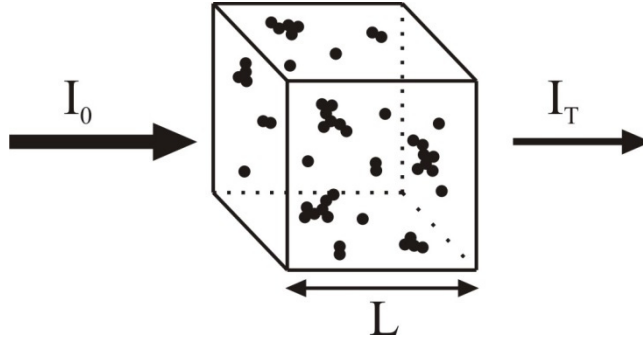
Figure 3.1
A schematic illustration of the Beer-Lambert law with light of irradiance I_0 incident on a volume of length L with dispensed soot particles, attenuating the light by scattering/absorption, resulting in transmitted light of irradiance I_T, with $I_T < I_0$.

Assuming that the Rayleigh criterion holds, see section 2.3, the absorption coefficient is given by

$$K_{abs} = \frac{\pi^2 E(m(\lambda))}{\lambda} N d_p^3.$$ (3.5)

Furthermore, assuming that the scattering contribution to the extinction is negligible in comparison with the absorption contribution, the scattering term in (3.4) can be disregarded. This assumption must be estimated for the measurement conditions at hand, while it may hold for some premixed flame it might not be valid for another flame which produces larger soot particles. Combining (3.1), (3.2) and (3.5) yields the following expression for the soot volume fraction

$$f_v = \frac{\lambda}{6\pi E(m(\lambda))} \ln\left(\frac{I_0}{I_T}\right) \frac{1}{L}.$$ (3.6)

Thus, by utilizing (3.6) the soot volume fraction can be measured using laser extinction. For cases where the scattering contribution is not negligible, it can usually either be measured or estimated and accounted for.

In the case of aggregated soot particles, assuming RDG theory holds, the absorption cross-section is that of a single primary particle multiplied by the number of primary particles in the soot aggregate, N_p.

There are some important points to consider for measurements of soot volume fractions by extinction. Since laser extinction is a line of sight technique the evaluated f_v will be an average value along the laser beam path and thus variations along this

path will not be detected. However, using more advanced (and complex) procedures, this can be circumvented [58-60], e.g. by measurements at different angles and/or positions and using the symmetry of the flame in the evaluation or by using LII in an imaging setup to attain the relative soot volume fraction along a line as was done in Paper III. As seen in (3.6), the soot volume fraction is inversely proportional to the absorption function, and therefore also affected by the value of the complex refractive index. Thus the inherent uncertainties of m, discussed in section 2.3, also propagate to the evaluated f_v, an important point to consider when evaluating soot volume fractions using extinction. Additionally, care should be taken to the influence of unwanted absorption by large molecules, like PAHs, since such absorption will lead to a lower I_T, which could be interpreted as a higher f_v if not accounting for the molecular absorption. By using laser wavelengths longer than ~700 nm, interferences by molecules can usually be avoided [61, 62], and see Paper X for a laser extinction study where this was investigated.

3.2.2   Elastic light scattering (ELS)

Elastic light scattering (ELS) is a commonly used technique for soot particle characterization. It has been used to extract complex refractive indices for soot as well as for particle sizing and measurements of soot aggregate structures, often in combination with other techniques, e.g. laser extinction or LII [15, 55, 63-67]. Additionally, see Paper III, V and IX for the use of ELS in conjunction with this thesis.

As for laser extinction, the principles of ELS are quite straight forward. When incident light hits soot particles a fraction of it will scatter off the particles. The amount of scattered light depends on several parameters e.g. detection angle, polarization of the light, size and concentration of the scatterers etc. Due to the small size of the soot primary particles the scattering can be assumed to follow Rayleigh theory, or RDG theory in the case of aggregated particles. The scattering theory presented here is based on more thorough descriptions found in [13, 37].

One important parameter for the scattering theory to be presented is the scattering wave vector, q, which is a function of the scattering angle, θ, i.e. the angle between the incident and scattered light. The scattering wave vector is expressed as,

$$q(\theta) = 2k\sin(\theta/2), \tag{3.7}$$

where $k = 2\pi/\lambda$ and λ is the wavelength of the scattered light. The inverse of the scattering wave vector, q^{-1}, can be seen as a kind of length scale of the scattering light, i.e. the probe length of a scattering experiment.

The scattered light intensity from a soot particle will be proportional to the differential scattering cross-section of that particle. Assuming that the light is scattered by an isolated spherical soot particle, the differential scattering cross-section can be expressed as

$$\frac{d\sigma}{d\Omega_p} = k^4 \left(\frac{d_p}{2}\right)^6 F(m). \tag{3.8}$$

If the scattering particle is an aggregated soot particle, assuming the aggregate consists of spherical primary particles in point contact, the differential scattering cross-section is instead described by the following expression

$$\frac{d\sigma}{d\Omega_{agg}} = N_p^2 \frac{d\sigma}{d\Omega_p} S(q), \tag{3.9}$$

where $S(q)$ is the structure factor of the aggregate. The structure factor has its name since it contains information about the structure of the scattering particle. Experimentally this structural information is converted to the scattering intensity varying with scattering angle. Depending on the size of the soot aggregate and the magnitude of the scattering wave vector, the structure factor is described by different expressions. To compare the length scale of the scattering to the aggregate size and determine what expression to use for the structure factor, the product qR_g is formed. The structure factor can then be expressed as follows for the Rayleigh, Guinier and power law regimes, respectively,

$$S(q) = 1 \qquad\qquad qR_g \ll 1, \tag{3.10}$$

$$S(q) = 1 - q^2 R_g^2 / 3 \quad qR_g \lesssim 1, \tag{3.11}$$

$$S(q) = C\left(qR_g\right)^{-D_f} \quad qR_g > 1, \tag{3.12}$$

where C is a coefficient determining the cutoff level between the Guinier and power law regimes. In his review [13], Sorensen shows that $C \approx 1$ for aggregates with $D_f \approx 1.8$, i.e. most flame generated soot aggregates. Utilizing (3.7)-(3.12), the scattered light intensity by a soot aggregate at a certain place in space, e.g. at a detector, can be expressed as

$$I_s = \eta I_0 N_{agg} \frac{d\sigma}{d\Omega}_{agg} = \eta I_0 N_{agg} N_p^2 k^4 \left(\frac{d_p}{2}\right)^6 F(m)S(q), \qquad (3.13)$$

where N_{agg} is the aggregate number density and η is a constant accounting for the solid angle, detection efficiency of the detector and various losses between the scattering particle and the detector etc. Using (3.13), or more refined versions of it, accounting for polydisperse distributions of aggregate and primary particle sizes, the structural parameters of soot aggregates can be evaluated from experimental ELS measurements, as described in [13].

For measurements of absolute scattering intensities it is important to know the polarization of the incident light since elastic light scattering in the Rayleigh regime is highly polarization dependent. Commonly laser light with a vertical polarization is used since this results in the most convenient geometry for the experimental setup, with the highest intensity of the scattered light in the horizontal plane. The total scattering cross-section in (3.3) can be derived from the differential scattering cross-section by integrating over all solid angles, and for the case of incident light with a vertical polarization the integral is expressed as

$$\sigma_{scat} = \int_0^{2\pi} \int_{-1}^{1} \frac{d\sigma}{d\Omega} \sin^2\phi \, d(\cos\phi) d\theta. \qquad (3.14)$$

To calibrate the scattering system for absolute measurements a gas with a known scattering cross-section is usually used, e.g. nitrogen.

There are some important considerations and restrictions for using elastic light scattering as a tool for characterization of soot particles. As for laser extinction measurements of soot, the uncertainty of the value of m will lead to uncertainties in scattering measurements as well. Further uncertainty is introduced due to polydispersity of the aggregate and primary particle sizes. Even though it is possible to incorporate a polydisperse size distribution in the evaluation, a specific distribution must be assumed. All the variables, i.e. for the polydisperse distributions and for the aggregate morphology, Eq. (2.1), lead to so many degrees of freedom that it becomes hard to find a single converging solution [67]. This can potentially be solved by combining ELS with other techniques, like LII, to reduce the degrees of freedom in the evaluation [66, 68].

3.2.3 Two-color pyrometry

Pyrometry is an optical technique for temperature evaluation from the Planck radiation of a black body or a gray body. By comparison of the theoretical expression for Planck radiation with the measured radiation, the temperature can be determined. Thus the temperature of soot can be measured and evaluated by utilizing Eq. (2.7). In Figure 3.2 the irradiance calculated using (2.7) is plotted as function of wavelength for a set of different temperatures to illustrate the difference in soot radiation for different experimental situations.
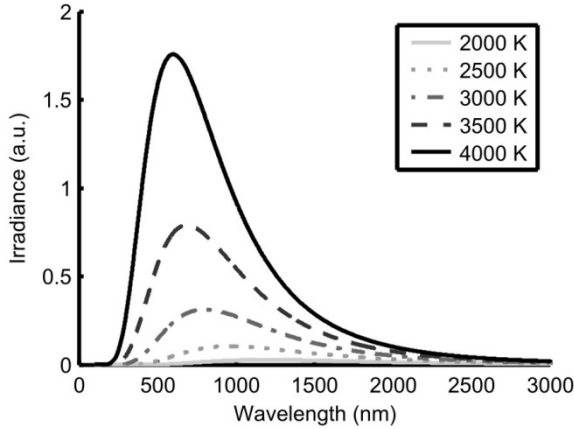
Figure 3.2
The irradiance of soot, calculated using Eq. (2.7), plotted as function of wavelength for different temperatures.

There are different methods to measure the soot emission and evaluate the temperature using pyrometry. Here a two-color procedure, frequently used in the work for this thesis, will be described. The two-color pyrometry method is based on measuring the soot emission at two different detection wavelengths, λ_1 and λ_2, and comparing the ratio of the signal at these wavelengths using the theoretical expression in (2.7) to evaluate a temperature. The ratio of the irradiance at the two wavelengths becomes

$$\frac{I(d_p,\lambda_1,T)}{I(d_p,\lambda_2,T)} = \varepsilon(d_p,\lambda_1)\frac{2\pi hc^2}{\lambda_1^5\left(\exp\left(hc/\lambda_1 k_B T\right)-1\right)} \bigg/ \varepsilon(d_p,\lambda_2)\frac{2\pi hc^2}{\lambda_2^5\left(\exp\left(hc/\lambda_2 k_B T\right)-1\right)}. \quad (3.15)$$

In order to simplify (3.15) it can be noted that for detection in the visible wavelength range and for typical soot temperatures

$$1 \ll \exp\left({hc}/{\lambda k_B T}\right). \tag{3.16}$$

Using (2.8) and (3.16), (3.15) can be simplified to the following expression for T,

$$T = \frac{hc}{k_B}\left(\frac{1}{\lambda_2} - \frac{1}{\lambda_1}\right)\Big/\ln\left(\frac{I_1}{I_2}\frac{E(m(\lambda_2))}{E(m(\lambda_1))}\left(\frac{\lambda_1}{\lambda_2}\right)^6\right), \tag{3.17}$$

where I_1 and I_2 are the irradiances at the two detection wavelengths. Thus (3.17) can be used to evaluate the soot particle temperature if the emission from the soot is measured at two different wavelengths. The largest strengths of this technique are that it is relatively simple to employ and that an absolute value of $E(m(\lambda))$ is not needed (the absolute value is very uncertain, as discussed in section 2.3). Assuming the ratio of $E(m(\lambda))$ to be one further simplifies the expression in (3.17). This is an assumption often used, but as discussed in Paper V, IX and X, this is a simplification more suitable for mature soot than for nascent soot due to seemingly stronger wavelength dependence of the absorption function for nascent soot.

In practice, a calibration source with a known emission spectrum is needed in order to calibrate the detection at the two wavelengths, see section 4.2.3.

3.2.4 Laser-induced incandescence (LII)

Laser-induced incandescence (LII) is nowadays a commonly used technique for visualization and characterization of soot, especially in combustion environments, and LII is also the main subject of this thesis. The first publication discussing the use of the LII process as a diagnostic technique was made by Weeks and Duley in 1974 [69], and three years later the process was described by Eckbreth [70], but this time as an interference on Raman scattering signals. In 1984 Melton published a work [71], where he thoroughly described the LII process and suggested how it could be used for evaluation of soot volume fractions and soot particle sizes using energy and mass balance equations, describing the different physical processes involved. All theoretical models today stem from the work by Melton, but with significant enhancements. The most refined of the LII models today is the one developed by Michelsen [32], where several physical processes not accounted for in other models are included. Reviews of laser-induced incandescence can be found in [9] and [10].

The basic principle of LII is that soot is rapidly heated by a high energy laser pulse, usually with a length of ~10 ns. If the pulse energy is high enough, the soot will reach peak temperatures of about 4000 K. As illustrated in Figure 3.2, the soot radiation intensity increases drastically with the increased temperature. This increased intensity

is detectable and the detected signal is thus the LII signal. After the laser pulse has passed, the soot will cool down to the ambient gas temperature and as the soot cools down, the LII signal will decay. Using a suitable detector e.g. a photomultiplier tube (PMT), the signal can be resolved in time and thus the signal decay can be measured. From the signal intensity the soot volume fraction, f_v, can be evaluated, while information about the soot particle diameter, d_p, can be extracted from the signal decay. Since the peak intensity is related to the soot volume fraction, these measurements can be applied in 2D using a laser sheet for heating the soot and a camera for detection, for example an intensified CCD (ICCD) camera. For quantitative measurements of f_v there is need of calibration, usually against a source with known soot volume fraction. This calibration source is commonly a laboratory flame where the soot volume fraction is known and has been measured with for example laser extinction. An alternative calibration procedure, using a calibration lamp, has been developed by Snelling et al. [72].

3.2.4.1 *Energy and mass balance*

The LII process is commonly described theoretically by the different physical mechanisms illustrated in Figure 3.3. Absorption of the laser light will increase the internal energy of the soot. The increased internal energy is associated with an increased temperature of the soot, which will cool down after the heating laser pulse has passed. The cooling occurs through heat conduction to the surrounding gas by molecules colliding with the soot, and through the increased thermal radiation. If the laser pulse energy is high enough, the soot will reach temperatures above ~3400 K at which the soot starts to sublime (see Paper IX), thus losing energy and mass. In addition to these processes, the theoretical model developed by Michelsen [32] also includes oxidation, melting, annealing and photodesorption of the soot.
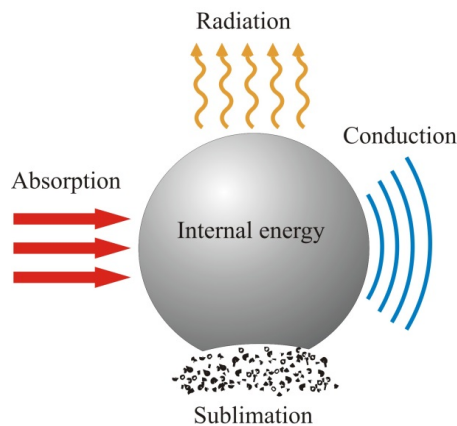

Figure 3.3
An illustration of the sub-mechanisms constituting the LII process that takes place when soot is heated by a high energy laser.

The energy balance of the LII process as described by Figure 3.3 can be described by the following expression, where $\dot{Q}$ denotes an energy rate for each of the included mechanisms,

$$\dot{Q}_{int} = \dot{Q}_{abs} - \dot{Q}_{cond} - \dot{Q}_{rad} - \dot{Q}_{sub}. \tag{3.18}$$

Studying (3.18) it can be noted that absorption, $\dot{Q}_{abs}$, is the only process increasing the energy of the soot. Using the absorption cross-section, σ_{abs}, described in section 3.2.1, the absorption of the laser light can be written as,

$$\dot{Q}_{abs} = \sigma_{abs} F \cdot g(t), \tag{3.19}$$

where F denotes the laser fluence (J/cm²) and $g(t)$ is the normalized temporal distribution of the laser pulse intensity. It can also be noted that since $\sigma_{abs} \propto d_p^3$, as described in section 3.2.1, the absorption is directly proportional to the soot particle volume, thus soot particles are volume absorbers. This means that if the soot is heated by uniform laser irradiance, it will reach essentially the same temperature even if the particle sizes differ, as long as the RDG theory is valid, see section 2.3.

The internal energy rate term corresponds to the energy transfer to and from the soot particles. It can be described by the following expression,

$$\dot{Q}_{int} = \frac{\pi}{6} \rho_s c_s d_p^3 \frac{dT}{dt}. \tag{3.20}$$

As discussed in section 2.3, there are some uncertainties associated with the density and specific heat since they both vary with temperature and soot maturity. Temperature dependent expressions for ρ_s and c_s, for example the ones suggested by Michelsen [32], can be used, resulting in a more complex expression due to the temperature varying with time. Additionally, when considering aggregated soot particles the rate term is multiplied by N_p, assuming the energy is distributed homogenously in the aggregate. This might introduce some errors for larger soot aggregates as the particles start to cool down, because of different cooling rates at different parts of the aggregates due to shielding effects, discussed in [73, 74] and investigated experimentally in Paper II.

An expression derived for the heat conduction in the free molecular regime [32], i.e. the soot particles are small compared to their mean free path, will be presented to give a qualitative understanding of the heat conduction process. There are also other models that are commonly used for the heat conduction, e.g. the McCoy and Cha

[75] and the Fuchs models [76, 77]. Of the current models the Fuchs model has been shown to be the most accurate. However, due to the Fuchs model being an iterative method, not having a closed form expression, it will not be presented here. Thus the heat conduction rate can be expressed as,

$$\dot{Q}_{cond} = \frac{\pi d_p^2 \alpha_T Z_{surf}}{N_A} \left(C_g - \frac{R}{2} \right) (T - T_g),$$ (3.21)

where α_T is the thermal accommodation coefficient, Z_{surf} is the collision rate of ambient gas molecules per unit surface area, N_A is the Avogadro constant, C_g is the heat capacity of the ambient gas, R is the universal gas constant, T is the soot temperature and T_g is the gas temperature. The thermal accommodation coefficient is a very important parameter for the heat conduction term. It is the probability for a molecule colliding with a soot particle to undergo energy exchange and thus carry away heat from the particle, and as seen in (3.21), it scales the whole expression. As the value of α_T for soot is very uncertain, with employed values ranging from 0.07 to 1.0 [78-82], and most likely there is also a variation with soot maturity (see for example Paper I and [83]), it inevitably leads to large uncertainties in the heat conduction term. Another important thing to note in (3.21) is that the heat conduction is proportional to the surface area of the soot, meaning that larger soot particles will cool down at a slower rate due to a smaller surface to volume ratio. The shielding effect mentioned in the previous paragraph has also been shown to have a significant impact, effectively decreasing the heat conduction, see [73, 74] for details about this. Additionally it should be mentioned that the heat conduction is highly pressure dependent, with higher pressure increasing the heat conduction rate. Readers are referred to [76, 77, 84] for more details about the heat conduction rate term.

The radiation as loss term is usually very small compared to the conduction term (on the order of a few percent [32]) and thus of small importance for calculation of the energy balance. However, the lower the pressure is, the higher the fraction of energy lost through radiation will be. Radiation from soot particles is described in section 2.3, and to get the energy rate term for a soot particle, (2.7) is integrated over all wavelengths (assuming a wavelength independent absorption function) and multiplied by the geometrical cross-section of the soot particle. This results in the following expression [32],

$$\dot{Q}_{rad} \approx \frac{199\pi^3 d_p^3 (k_B T)^5 E(m(\lambda))}{h(hc)^3}.$$ (3.22)

By studying (3.22) it can be noted that the radiation from soot is proportional to the particle volume. Thus soot particles are not only volume absorbers, as stated previously. They are also volume emitters, as an effect of Kirchhoff's law.

At laser fluences around 0.14 J/cm² (at a laser wavelength of 1064 nm) the soot starts to sublime (see Paper IX) forming gas-phase carbon, mostly as C, C_2 and C_3 [32]. Thus the sublimation of soot results in loss of both energy and mass. The energy rate expression can be written as [85],

$$\dot{Q}_{sub} = -\frac{\Delta H_v}{M_v}\frac{dm_p}{dt},$$ (3.23)

where ΔH_v is the heat of sublimation, M_v is the molecular weight of soot vapor and m_p is the mass of the soot particle. Additionally, the mass rate can be expressed as [85],

$$\frac{dm_p}{dt} = -\pi d_p^2 N_v \frac{M_v}{N_A},$$ (3.24)

where N_v is the molecular flux of sublimed carbon. Since sublimation occurs at high laser fluences it is likely that other processes altering the soot also take place, [32, 86, 87]. Thus it is hard to predict the behavior of the LII process at fluences larger than ~0.14 J/cm², called the high fluence regime. Consequently, the fluence region below ~0.14 J/cm² is called the low fluence regime. The exact transition point between these two regimes depends on flame temperature and soot properties and the threshold value of ~0.14 J/cm² was established for the premixed ethylene/air flames studied in Paper IX. From (3.23) and (3.24) it can be noted that, as for the heat conduction term, the sublimation is also proportional to the surface area of the soot particles.

Using the equations for energy and mass balance, it is possible to model the LII process by solving the energy and mass balance equations for $T(t)$ and $d_p(t)$, i.e. soot particle temperature and diameter as functions of time. Using these time-dependent functions and (2.7), the LII signal from an aggregated soot particle can be calculated as,

$$S_{LII} = N_p \pi d_p^2 \int_0^\infty \eta(\lambda)\left(I(d_p,\lambda,T) - I(d_p,\lambda,T_g)\right)d\lambda,$$ (3.25)

where $\eta(\lambda)$ is a coefficient accounting for the spectral sensitivity of the detection system. By fitting of the modelled time-resolved signal and temperature to

experimentally measured ones it is possible to evaluate for example soot particle sizes or $E(m)$.

3.2.4.2   LII signal interpretation

Displayed in Figure 3.4 are two experimentally measured LII signals. These have been measured at two different heights in a flat premixed ethylene/air flame burning on a McKenna burner (described in section 4.1.1) at $\phi = 2.1$. The temporal profile of the heating laser has been plotted together with the LII signals to give a quantitative comparison of the LII signal length and the laser pulse length. A typical LII signal at atmospheric pressure is some hundred nanoseconds up to around 1-2 microseconds long, depending mainly on the soot particle sizes. As can be seen in Figure 3.4, the signal from the soot at 8 mm height above burner (HAB) has a significantly faster decay than the signal from the soot at 14 mm HAB. This is primarily due to the primary particle diameters at 14 mm HAB being larger than at 8 mm HAB. Evaluation by TEM resulted in diameters of ~12 nm and ~8 nm at 14 mm HAB and 8 mm HAB, respectively, see Paper I. There is also an influence of shielding due to particle aggregation at 14 mm HAB effectively increasing the signal length, and some influence from the different soot peak temperatures and ambient gas temperatures at the two heights, see Paper I. By analyzing the time-resolved LII signals using numerical LII models there is thus potential for evaluation of several soot properties. To simplify the evaluation it is preferable that the measurements were conducted in the low fluence regime, since then the sublimation and other processes occurring at higher fluences can be neglected.
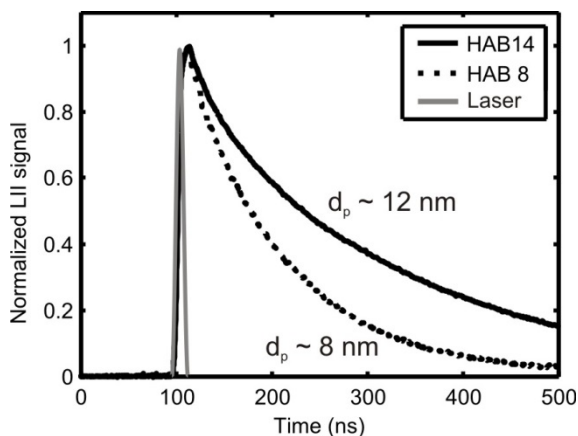

Figure 3.4
A plot of two experimentally measured, normalized and time-resolved LII signals at 8mm and 14 mm heights above burner (HAB) in a flat premixed ethylene/air flame at $\phi = 2.1$. The heating laser (1064 nm, top-hat at 0.14 J/cm^2) temporal profile can be seen in gray. The primary particles diameters are about 12 nm and 8 nm at 14 mm and 8 mm HAB respectively.

In the work by Melton [71] the gated LII signal (over the peak of the signal) dependence on particle number concentration and size is given as,

$$S_{LII} \propto N d_p^{3+0.154 \cdot 10^{-6}/\lambda_{det}}, \tag{3.26}$$

where λ_{det} is the detection wavelength in meter. Studying (3.26) it can be noted that the gated LII signal is approximately proportional to the soot volume fraction as,

$$S_{LII} \propto N d_p^3 \propto f_v. \tag{3.27}$$

This approximation is commonly used for 2D measurements of soot volume fractions by utilizing a laser sheet for heating the soot and then the induced soot incandescence is imaged onto a camera with a suitable gating time to collect the LII signal. Thus, by calibration towards a source with known f_v, every pixel value in the camera can be related to a soot volume fraction value,

$$f_v = C_{cal} \cdot S_{LII}, \tag{3.28}$$

where C_{cal} is the calibration coefficient. It can be noted that the longer the detection wavelength is, the smaller the error induced by the approximation in (3.27) is. In an extensive investigation by Bladh et al. [88] the relation between the soot volume fraction and gated LII signal was investigated and it was found that when using (3.27), the error is minimized if using as short detection gate and long detection wavelength as possible.

When studying the theory presented in the previous section it becomes clear that the LII signal has nonlinear laser power dependence. Presented in Figure 3.5 is a plot of the normalized measured peak LII signal for different heating laser fluences at 1064 nm, commonly denoted as a fluence curve, in a flat premixed ethylene/air flame at $\phi = 2.1$ and at 14 mm HAB. The fluence curve shows a steep signal gradient in the region up to ~0.3-0.4 J/cm², where it transitions into a plateau region at fluences above ~0.4 J/cm². This is a typical fluence curve shape, and it can be explained by the processes described in section 3.2.4.1. The steep gradient occurs due to the absorption being the dominating process, in fact the signal can be seen to follow the T^5 dependence in (3.22) at lower laser fluences where the sublimation process still has minor influence. As the sublimation becomes more and more prominent with increasing laser fluence, the signal levels off and transitions into a plateau behavior as the soot peak temperature around 4000 K is reached.
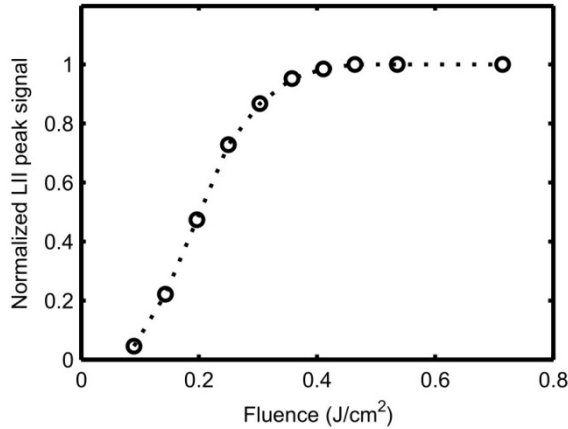
Figure 3.5
Experimentally measured peak LII signal plotted as function of heating laser fluence and normalized to the measurement point at the highest fluence. Such a plot is commonly denoted as an LII fluence curve. The heating laser operated at a wavelength of 1064 nm and detection was made over a 24 nm wide wavelength band centered at 684 nm. The measurement was made at 14 mm HAB in in a flat premixed ethylene/air flame at $\phi = 2.1$.

If the signal is gated over the peak, as for a 2D measurement of f_v, instead of measured at the peak, the sublimation and conduction processes will have large influence on the shape of the fluence curve. Then also the spatial intensity profile of the heating laser will have a large impact on the shape. Illustrated in Figure 3.6 are three common laser spatial intensity profiles: the Gaussian beam, Gaussian sheet and top-hat profiles.
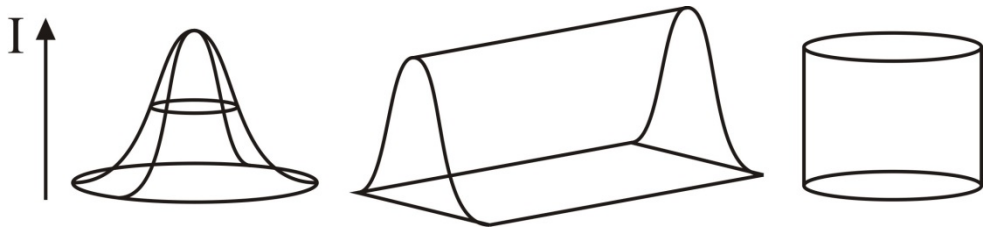
Figure 3.6
An illustraion of three different laser beam spatial intensity profiles. From the left, Gaussian beam, Gaussian sheet and top-hat profiles.

Modelled LII fluence curves corresponding to the laser intensity profiles in Figure 3.6 are plotted in Figure 3.7. As can be seen, the Gaussian sheet is the only laser profile giving rise to a plateau region for the corresponding fluence curve. This can be explained by a balance between the loss of signal in the center of the laser profile due

to sublimation and an increase of signal from the "wings" of the Gaussian sheet with increasing laser fluence.

Figure 3.7
Modelled LII signal as function of average heating laser fluence, i.e. fluence curves, using a detection gate time of 100 ns over the peak of the signal and $d_p = 10$ nm, presented for three different laser beam spatial intensity profiles. The curves are normalized to their peak values and the laser beam spatial profiles used were a Gaussian beam, a Gaussian sheet and a top-hat, as indicated in the figure. The original modeling and figure are presented in [89].
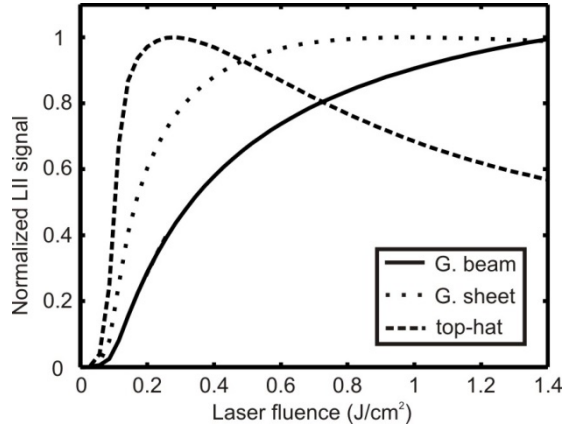
For evaluations of f_v it is desirable to perform the measurements in a fluence regime corresponding to a plateau region, since by doing so, small fluctuations in laser energy (e.g. due to absorption along the laser beam) will have minor impact on the evaluated soot volume fraction. Thus a Gaussian sheet laser spatial profile should be used for measurements of f_v when using gated detection, in accordance with the fluence curves presented in Figure 3.7.

3.2.4.3   Main uncertainties in LII

As with all measurement techniques, there are both strengths and weaknesses with LII as a diagnostic technique. The main sources for error in LII will be discussed here.

The most common application of LII is for measurements of soot volume fractions, in which the LII signal is usually assumed to be proportional to the soot volume fraction as described in the previous section. As also mentioned, keeping the gate time as short as possible and the detection wavelength as long as possible will minimize the errors induced by the assumption of proportionality. However, the longer the detection wavelength is the larger the influence of background radiation from the flame is and the shorter the gate is the weaker the signal. Thus a balance has to be found, which of course depends on the measurement conditions at hand. Additionally, as discussed in conjunction to Figure 3.7, errors induced by laser energy variations can be minimized by measuring at laser fluences corresponding to a plateau

34

region. The main uncertainty can however be traced back to the calibration. Assuming a laboratory flame is used as calibration source, all the uncertainties from the measurement of f_v in the calibration source are transferred to the LII measurement. Presuming laser extinction was used to determine the absolute value of f_v (which is commonly the case) it is the uncertainties of this technique (discussed in section 3.2.1) that are carried over to the LII measurement of the soot volume fraction. Most notable are the large uncertainties connected to the value of the complex refractive index, as discussed in section 2.3. Furthermore, any variations of the soot particle characteristics between the calibration flame and the measurement target that lead to differences in the induced signals, such as variations of the complex refractive index or level of maturity, will also lead to uncertainties in the evaluated soot volume fractions.

Evaluation of soot primary particle diameters and other soot properties from the decay of the LII signal is prone to large uncertainties. To reduce the uncertainties and in order to know what can be expected from evaluation of time-resolved LII measurements, here are some important considerations:

1. The preferred laser spatial profile for these measurements is usually a top-hat, to ensure that all soot particles are heated to the same temperature. However, the experimental laser profile is never a perfect top-hat since there will always be deviations due to diffraction patterns etc. This means that the soot will be unevenly heated, which due to the T^5 term in (3.22) means that the emitted signal will be skewed towards higher temperature than the average temperature, as long as the maximum temperature of ~4000 K is not reached. At this limit, when major sublimation occurs, variations in the laser profile will instead affect the decay time, since regions of the laser profile with higher laser fluence will induce more sublimation and thus shorter signals. An extensive study on this subject has been made by Michelsen et al. [90].

2. The soot primary particles and aggregate sizes have polydisperse distributions, meaning that the emitted signal is dominated by the emission of the larger particles due to the soot particles being volume emitters. Furthermore, increasing aggregation leads to an increased shielding effect. Thus, if assuming monodisperse distributions, the evaluated particle size will be larger than the true average size. This effect is more pronounced the longer after the peak signal the evaluation is done since the smaller particles have shorter decay times. Hence the larger the time-delay to the peak signal is, the more the signal is dominated by the large soot particles.

3. It is very challenging to achieve agreement between experimental and modelled signals at laser fluences above the sublimation threshold. At these fluences the sublimation (3.23) and other not so well characterized processes must be modelled, e.g. photodesorption and annealing. Thus the high fluence regime is usually avoided.

4. The thermal accommodation coefficient, α_T, which scales the conduction term (3.21) and thus has a large influence on the evaluation of the signal decay, is one of the larger uncertainties in the evaluation. Due to the large spread of reported values of α_T, discussed in section 3.2.4.1, there is inevitably also a large uncertainty in the parameters evaluated from the signal decay, e.g. soot particle sizes.

5. Through the uncertainty in the value of $E(m(\lambda))$ there is an inherent uncertainty in the absorption term (3.19). This is commonly avoided in LII model evaluations by estimation of the soot peak temperature by two-color pyrometry and matching the modelled peak temperature to the measured one. Even though this method avoids the absolute value of the absorption function, it suffers from the uncertain wavelength dependence of $E(m(\lambda))$ through the ratio seen in (3.17).

Further improvement of the evaluation can be achieved by measuring the soot particle size at some of the LII measurement points with another technique e.g. TEM, as was done in Paper I, and use this size as a calibration value.

4 Experimental equipment and considerations

When conducting LII measurements, or basically any other laser diagnostic measurements, the experimental setups are commonly quite complex. In this chapter the most central experimental equipment for this thesis will be described and in addition some important experimental considerations will also be discussed.

4.1 Soot generation

As explained in chapter 2, the fundamental prerequisite for soot production is fuel rich combustion of some hydrocarbon, effectively making it relatively easy to generate soot. However, generating soot under controlled conditions and achieving a stable and reliable sooting source is much more challenging. For this purpose there are different kinds of soot generators. There is for example a Swiss company named Jing [91], which manufactures different models of cold soot generators called CAST (Combustion Aerosol STandard), these have however not been used in the work for this thesis. Other commonly used sources are different kinds of laboratory burners, burning either liquid or gaseous fuels. Within the LII community there are three different gas burners that have been designated as target burners together with standard operating conditions for which ethylene is burnt with air as oxidizer [10, 92]. Two of these burners, the McKenna burner and the Gülder burner, have been used in this work and will be described in the following sections.

4.1.1 The McKenna burner

The McKenna burner is manufactured by Holthuis & Associates [93] and is a gas burner used to produce flat premixed flames. In Figure 4.1 a photograph of a McKenna burner is displayed together with a cutaway view to see how it is constructed. With the cutaway view in mind, the burner construction can be explained as follows. The fuel/oxidizer mixture is supplied to the center of the burner through a pipe connected at the bottom. This gas mixture then exits through a central

porous plug with a diameter of 60 mm. Just outside of the central plug there is a second coannular porous plug to produce a shielding co-flow around the central plug. The gas for the co-flow is also supplied through a pipe connected to the bottom of the burner. This co-flow is used to protect the flame from fluctuations induced by air movements in the surroundings e.g. from ventilation systems. As can be seen in the sketch in Figure 4.1 there is a thin piping connected to the central plug for cooling water which is used to keep the porous material from melting and at a constant temperature. Seen in the photograph is a stainless steel flame stabilizer with a diameter of 60 mm. This is placed centered above the burner to achieve a nice and stable flame suitable for measurements. The burner is manufactured in different versions; there are McKenna burners with either steel or bronze porous plugs and there is also a low-pressure version of the burner, meant for operation at pressures below atmospheric pressure.
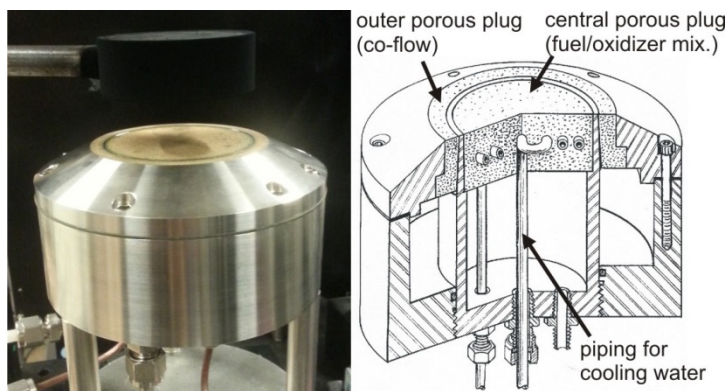

Figure 4.1
To the left there is a photograph of a bronze plug McKenna burner and to the right is a cutaway illustration of the burner.

The premixed target flame within the LII community [10, 92] is a premixed ethylene/air flame burning on a bronze plug McKenna burner at $\phi = 2.1$. This value can however easily be changed by changing the ethylene/air ratio if a fuel richer or leaner flame is wanted. The ethylene/air mixture should have a flow rate of 10 L/min (at 273 K and 1 atm) and the stabilization plate should be placed with its lower edge at 21 mm height above the burner surface to produce the premixed and laminar standardized flame. Even though a co-flow gas is not specified for the standardized case, a co-flow is commonly used to achieve better stability. The standardized flame is clearly sooting and has a bright yellow luminosity, see Figure 4.2. The reaction zone can be found about 1-2 mm above the burner surface and is recognizable as a thin blue disc (not visible in Figure 4.2 due to the soot incandescence). The soot starts to form above the reaction zone and grows with height above burner (HAB), as described by Figure 2.2, with soot aggregates starting to form at about 10-12 mm

HAB, see Paper I. The soot growth also results in larger primary particle sizes and higher soot volume fractions with increasing flame height, see Paper I and Paper X. The flame temperature peaks at 4 mm HAB where it is ~1750 K and then decreases when moving towards the flame stabilizer at 21 mm HAB, see section 5.1.1 and Paper I and III for more information about the flame temperature. In addition to the settings for the standardized flame it should also be noted that a standard height for measurements has been defined at 12 mm HAB.

Although the standardized flame does not have a defined co-flow it is common to use either a co-flow of air or nitrogen to shield the flame from wind whiffs due to movements in the surroundings, effectively leading to a more stable flame. For the measurements in premixed flames on McKenna burners in this thesis, the flow speed of the co-flow has been matched to that of the cold flow speed of the central ethylene/air mixture. In Figure 4.2 two photographs of $\phi = 2.1$ flames are presented, one with a nitrogen co-flow and the other with a co-flow of air. As seen in the photographs, the choice of co-flow gas has an impact on the flame. While the visible flame width with a co-flow of nitrogen is 25 mm at 10 mm HAB, it is 27.5 when using a co-flow of air. This difference can be explained by an outer oxidation of unburned products (mainly soot, carbon monoxide and hydrogen) when using air as co-flow, which gives rise to the yellow luminosity seen also around the stabilizing steel plate, while the nitrogen co-flow instead rapidly cools the soot leaving the flame. For investigation and further discussion about the influence of co-flows on McKenna burner flames, see section 5.1.1 and Paper III.
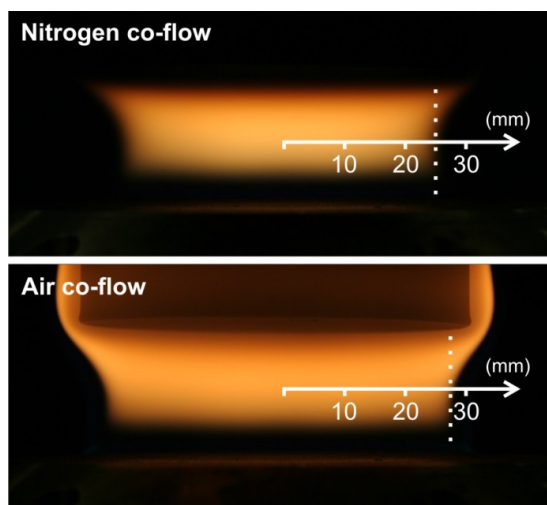

Figure 4.2
Ethylene/air flames burning on a McKenna burner at $\phi = 2.1$ where the top flame has a co-flow of nitrogen and the bottom one has a co-flow of air. The flow speed of the co-flow is matched to that of the cold flow of the ethylene/air mixture. The scale shows the visually evaluated flame edge position at 10 mm HAB, see Paper III.

Flat premixed flames are often referred to as one-dimensional, meaning that variations are seen only along the vertical axis while the conditions are constant along the radial axis. As a result of the one-dimensionality it is possible to follow the soot formation with HAB, where the soot forms low in the flame and then grows with height. This makes it possible to conduct measurements of soot at different stages in the soot formation process by probing different flame heights, see Paper I, III, V, VI, IX and X for studies in flat premixed ethylene/air flames. The one-dimensionality of the flames should however be considered as an approximation, since there are some variations with radial position. While the temperature is essentially constant in the central parts of the flame it either increases or decreases at the edges depending on if air or nitrogen is used as co-flow. Furthermore, some variation has also been seen of soot particle sizes and soot volume fractions. See section 5.1.1, [94] and Paper III for details on the flame characteristics. As a result of the stability and the flame being well characterized it is often used as calibration source for absolute measurements of soot volume fractions, see for example Paper IV and VIII.

4.1.2   The Gülder burner

The Gülder burner is a gas burner mainly used to produce stable laminar diffusion flames for soot studies [66, 95]. The fuel is provided through a central fuel tube with an inner diameter of 10.9 mm. There is a coannular air nozzle with an inner diameter of 88 mm surrounding the fuel tube, for providing a stabilizing air flow around the flame. Prior to exiting the nozzle, the air passes a layer of glass beads (5 mm diameter) placed between two porous metal discs to achieve a stable air flow without instabilities. A photograph of the burner is displayed to the left in Figure 4.3.
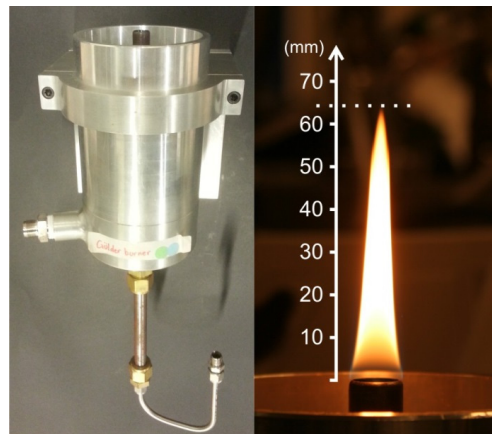

Figure 4.3
A photograph of the Gülder burner is displayed to the left in the figure and to the right is a photograph of the standardized ethylene diffusion flame together with a scale indicating the visible flame height at 64 mm.

The standardized flame is attained by providing an ethylene flow at 0.194 L/min (at 294 K and 1 atm) and an outer air flow of 284 L/min. This should optimally result in a laminar diffusion flame with a visible flame height of ~64 mm, as depicted to the right in Figure 4.3. However, the visible flame height may vary a few millimeters depending on for instance the absolute value of the surrounding atmospheric pressure. A position at the center of the flame and at a height of 42 mm above the tip of the fuel tube has been defined as the standard measurement position and here the soot volume fraction has been shown to stay at a relatively constant value of about 4.0 ppm over 3 mm at a flame width of ~5 mm [72]. The gas temperature at this position has been measured to ~1700 K [96].

While it is not possible to follow the soot formation in a Gülder burner diffusion flame in the same manner as for a premixed McKenna burner flame, the diffusion flame has other advantages for measurements. It produces more soot and there are positions where the generated soot is of a more mature character than in premixed flames [87], making these flames more suitable for some studies. In connection to this thesis the standardized Gülder burner flame was used as measurement target for the study presented in Paper VII, where gas heating effects from laser heated soot were studied, which required a heavily sooting flame.

4.2 Two-color LII setup

A sketch of a typical setup for two-color LII, as it has been applied in much of the work in this thesis, is presented in Figure 4.4. In short the setup typically consists of a Q-switched Nd:YAG laser (Quantel Brilliant B) operating at its fundamental wavelength of 1064 nm and with a repetition rate of 10 Hz. The laser beam is guided by mirrors to the measurement location at which it has a top-hat spatial intensity profile, achieved by a relay imaging system. The pulse energy is adjusted by an attenuator system and the beam profile is monitored by a beam profiler CCD camera (WinCamD-UCD15) while the pulse energy is measured by a pyroelectric laser power meter (Ophir PE25BB-DIF). The signal is detected by PMTs (Hamamatsu H6780) at two different wavelength bands by using band-pass filters (Semrock BrightLine).
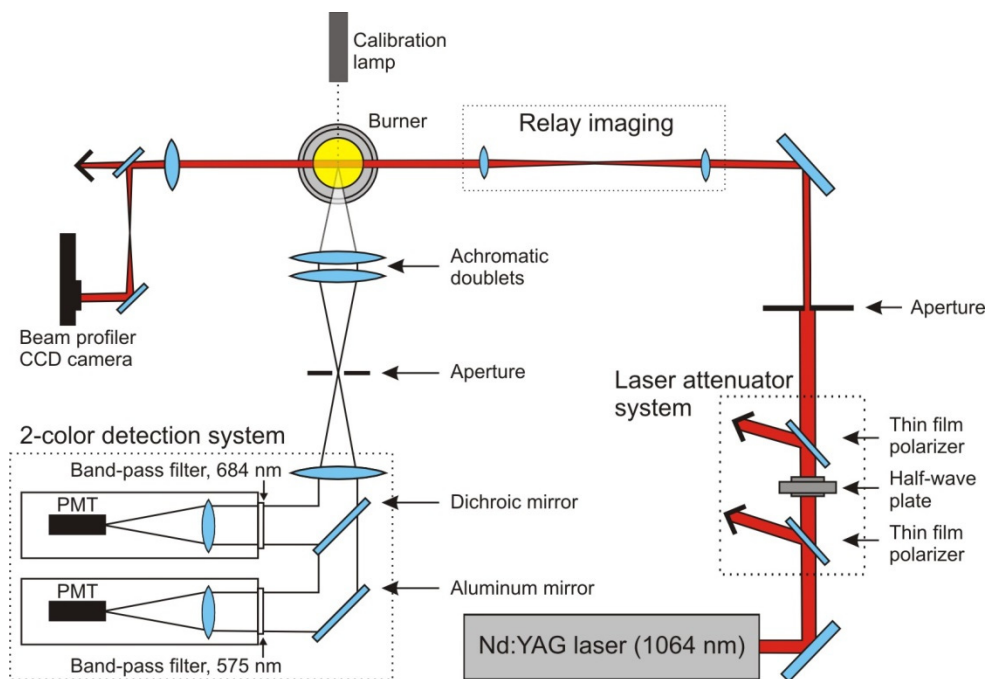
Figure 4.4
A sketch of a typical two-color LII setup as it has been arranged in much of the work constituting this thesis.

In the following sections separate parts of the two-color LII setup will be described in more detail. Additionally, important points to consider will also be discussed to elucidate specific details and choices.

4.2.1 Laser considerations

When choosing laser for the measurements there are several considerations to take into account so that the uncertainties and errors are minimized while the signal-to-noise ratio is maximized. Beginning with the wavelength of the laser, it might seem like a choice of short wavelength would be preferable due to the soot absorption having an inverse proportionality to wavelength, as seen in Eq. (3.5). However, with modern lasers it is not a problem to reach energies far higher than what is needed for LII, even in the long visible and infrared wavelength regions. In addition to the soot having high absorption efficiency at short wavelengths there are numerous molecular species in flames that absorb at wavelengths below ~700 nm [61, 62], most notable are PAHs, discussed also in Paper X. Using laser wavelengths below ~700 nm will thus result in laser induced fluorescence (LIF) from these molecules, which may interfere with the LII signal. Hence it is preferable to utilize laser wavelengths above

700 nm for LII measurements, making Nd:YAG lasers with a fundamental wavelength of 1064 nm a suitable choice, not only because of the wavelength, but also the availability, cost and high output power. A considerable drawback of working with laser light at 1064 nm is that it is not visible to the naked eye. This makes alignment of the setup more complicated than when working with visible laser wavelengths. Furthermore the laser light at 1064 nm is an eye safety hazard, not only because it is invisible, but because the light is not absorbed by the cornea and lens in the eye and thus this radiation may cause irrevocable damage to the retina.

The spatial intensity profile of the laser is also of importance for the measurements, as discussed in section 3.2.4 and in [90]. For time-resolved two-color measurements a top-hat profile is preferable as all particles will reach essentially the same peak temperature (assuming $E(m)$ is the same) since the soot particles are volume absorbers, as discussed in section 3.2.4. An experimentally acquired image of a top-hat profile from a two-color LII setup like the one displayed in Figure 4.4 can be seen in Figure 4.5. The presented profile is the one used for the measurements in Papers V and IX. As can be seen in Figure 4.5, the profile exhibits some variations (standard deviation of 13.5%) and hence it is not a perfect top-hat profile with the same laser fluence at every position, which is not experimentally achievable. The variations in the profile come for example from lens aberrations and diffraction patterns originating from the sharp edges of the apertures, as seen in the lower left part of Figure 4.5.
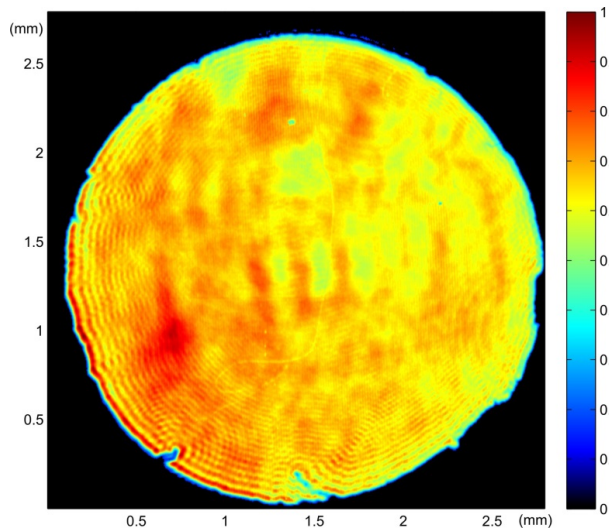

Figure 4.5
An image taken with a beam profiler camera of the experimentally acquired top-hat intensity profile of the heating 1064 nm laser in Papers V and IX. The dimensions are indicated by the X and Y-axes and the intensity has been normalized to 1.

The typical pulse length of pulsed Nd:YAG lasers at ~10 ns is suitable for LII measurements at atmospheric and lower pressures. This is due to the induced LII signals at these pressures having a considerably longer duration (~1 μs at atmospheric pressure and even longer at lower pressures) than the laser pulses. However, at elevated pressures, tens of bars over atmospheric pressure, the LII signal length is significantly shorter and comparable to a nanosecond laser pulse. This means that picosecond laser pulses may be preferable instead of nanosecond laser pulses in order to simplify the evaluation of the LII signal decay [97]. This should be taken into consideration if conducting time-resolved LII measurements in for example the cylinders of internal combustion engines.

An additional point to consider when discussing the temporal behavior of the laser is the spatiotemporal behavior. Depending on radial position in the laser profile, the temporal profile of the laser light may differ, as discussed in [98]. This is a phenomenon arising due to the unstable resonators used in many Q-switched Nd:YAG lasers, resulting in different temporal profiles and delays of up to ~10 ns between the center and edges of the laser profile. As a result, unwanted errors might be induced in measurements where high temporal sensitivity is needed if this is not taken into consideration, for example by discarding the outer regions of the laser spatial profile.

4.2.2   Laser beam optics

The laser attenuator system seen in Figure 4.4 is used for adjustments of the laser pulse energy and consists of two thin film polarizers and a half-wave plate. The laser beam is first ensured to be linearly polarized before passing the half-wave plate by placing one of the thin film polarizers in front of the half-wave plate while the other one is placed on the other side. Thus by rotating the half-wave plate, the polarization of the linearly polarized laser light incident on the second thin film polarizer will be turned. This effectively changes the transmitted pulse energy depending on the rotation angle between the half-wave plate and the second thin film polarizer. By using an attenuator setup like this instead of e.g. changing the flashlamp to Q-switch delay for adjusting the pulse energy, the temporal and spatial characteristics of the laser pulses are maintained.

The relay imaging system in Figure 4.4 is used to achieve a top-hat spatial profile of the laser beam, as displayed in Figure 4.5. This is done by using an aperture to cut out the central section of the laser profile with close to homogenous intensity distribution and relay imaging this section to the measurement location. Thereby also solving the potential problem arising from a spatiotemporal laser profile as discussed in the previous section. Thus the size of the achieved spatial profile is defined by the size of the aperture and magnification of the imaging system. The benefit of using a relay imaging system with two lenses instead of imaging with a single lens is that the

light rays stay parallel. Nevertheless, the top-hat profile will deteriorate with increasing distance from the image plane. This effect can be countered through elongating the depth of field by using long focal lengths of the imaging lenses.

4.2.3 Detection system

The signal collection is achieved by imaging of the measurement position by a combination of two achromatic doublets onto an aperture, which size thus delimits the probe volume. To make it possible to detect the signal at two different wavelength bands the aperture is followed by an imaging system of achromatic doublets including a dichroic mirror to separate the signal into two paths, see Figure 4.4. The wavelength bands are determined by two band-pass filters and the signal is collected onto PMTs connected to a 1-GHz, 4-channel digital oscilloscope (LeCroy Waverunner 104MXi) capturing and storing the signals. Implementing the signal collection this way ensures that the signal at the two wavelengths originates from the same volume. Furthermore, it is simple to add additional detection wavelengths by adding additional dichroic mirrors, filters and PMTs, as was done in Paper V and IX for detection of scattering at 532 nm.

A calibration of the two-color detection system is required for evaluation of soot temperatures by pyrometry. For this a calibration lamp (Labsphere IES) with a known emission spectrum is needed. This lamp is placed so that the emitted light is directed straight into the signal collection system, see Figure 4.4. The calibration and temperature evaluation is then carried out according to the following description. If the signals detected at the two wavelength bands by the PMTs are written as S_{1m} and S_{2m}, then the irradiance from the measurement position at the two detection wavelength bands can be expressed as,

$$I_1 = C_1 S_{1m}, \tag{4.1}$$

$$I_2 = C_2 S_{2m}, \tag{4.2}$$

where C_1 and C_2 are calibration constants for the detection efficiency. These calibration constants can then be combined into one as,

$$C = \frac{C_1}{C_2} = \frac{I_1 S_{2m}}{I_2 S_{1m}}. \tag{4.3}$$

Utilizing Eq. (3.17) in combination with (4.3), the temperature can be evaluated as,

$$T = \frac{hc}{k_B}\left(\frac{1}{\lambda_2} - \frac{1}{\lambda_1}\right)\Big/\ln\left(C\,\frac{S_{1m}}{S_{2m}}\frac{E(m(\lambda_2))}{E(m(\lambda_1))}\left(\frac{\lambda_1}{\lambda_2}\right)^6\right). \qquad (4.4)$$

4.2.4 Laser monitoring

The laser pulse energy and spatial intensity profile were monitored by a pyroelectric laser power meter and a beam profiler CCD camera, respectively. To measure the pulse energy is a straight forward procedure, where the power meter is inserted in the beam path during the measurement and withdrawn afterwards. During measurements a reflex of the laser pulses is monitored by a fast photodiode (EOT ET-3500, rise/fall time is 25 ps) connected to the oscilloscope for collecting the time-resolved laser pulse, which can be used as input in the evaluation of the time-resolved LII signals and also to reveal any variations of the pulse energy.

For monitoring of the spatial profile the position along the laser beam at which the profile is to be investigated must be imaged onto the CCD chip of the beam profiler camera. This is achieved by imaging with a single lens as shown in Figure 4.4. Due to the high energy of the laser pulses, the laser light must be attenuated before reaching the beam profiler sensor. This is done by utilizing glass windows in series to reflect fractions of the laser light until low enough pulse energy is achieved for the beam profiler sensor, as illustrated in Figure 4.4.

5 Results

The main findings of the work in this thesis are summarized in this chapter. To begin with, the results of measurements in premixed ethylene/air flames burning on McKenna burners will be presented. This is followed by the results from studies of processes directly affecting the LII signals and then the chapter is ended with a summary of the results from applied LII measurements.

5.1 Measurements in flat premixed ethylene/air flames

Much of the experimental work with LII in this thesis is based on measurements in flat premixed ethylene/air flames burning on McKenna burners. The main reasons for this are that they are stable flames and also offer the possibility to separately measure on soot at different stages in the soot formation process, i.e. from nascent to mature soot. This section summarizes the results found in Paper I, III, V, VI, IX and X, where different soot studies have been conducted in flat premixed flames.

5.1.1 Characterization of flat premixed ethylene/air flames

The flat premixed ethylene/air flames burning on McKenna burners are well characterized, see for example [51, 56, 65, 81, 94] in addition to the papers summarized here. A significant effort in the characterization of these premixed flames was done in Paper III, a study stimulated by the work of Migliorini et al. [94], where the commonly assumed one-dimensionality of the flames was investigated.

As the premixed ethylene/air flame at $\phi = 2.1$ has been denoted as a standard case within the LII community, see section 4.1.1, this is also the most studied flame. However, also other equivalence ratios have been used. Fuel richer flames with higher ϕ can be of interest when heavily sooting flames are desired, for example to achieve strong signals [65, 99]. There are also cases when flames with lower ϕ are of interest, for example in Paper VI where low-sooting flames at lower ϕ were used for studies of nascent soot. The visual sooting limit was found at $\phi = 1.75$, while the detection limit for LII (using the LII setup described in Paper VI) was found to be $\phi = 1.77$. For a visual comparison of premixed ethylene/air flames on a McKenna burner at

different equivalence ratios starting at the sooting limit, see Figure 5.1. In the low-sooting flames at $\phi < 1.9$ the reaction zone can clearly be seen as a thin blue/green disc above the surface of the burner in the images. The blue/green color comes from the chemiluminescence of CH and C_2 formed in the reaction zone [100].
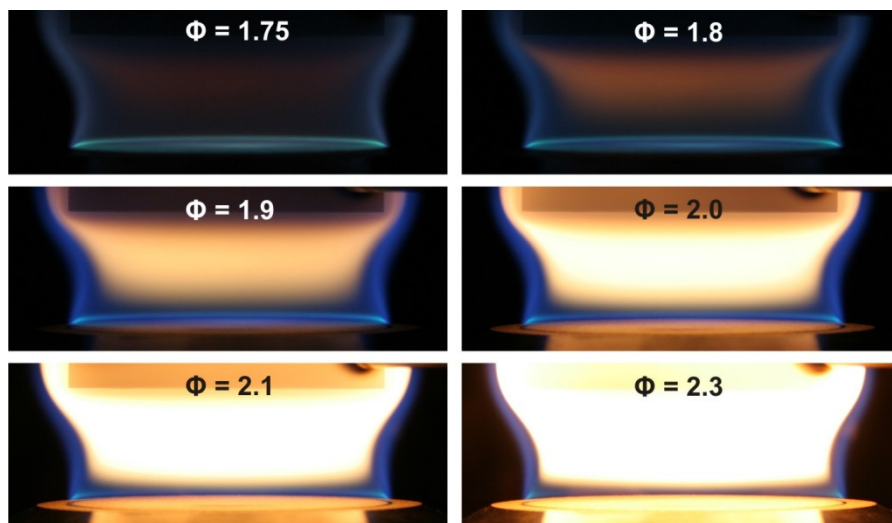

Figure 5.1
A comparison of premixed ethylene/air flames on a McKenna burner at different equivalence ratios with a co-flow of air at a flow speed equivalent to the cold flow speed of the ethylene/air mixture.

Measurements using various measurement techniques have been conducted at different HAB, especially in the standardized ethylene/air flame at $\phi = 2.1$. The flame temperature, mean primary particle diameter and soot volume fraction as functions of HAB are displayed in Figure 5.2. The temperature, measured by rotational coherent anti-Stokes Raman spectroscopy (CARS) of N_2 [101-103], can be seen to have a very steep gradient just above the surface of the burner. This gradient can be explained by the water-cooled porous plug, which is maintained at a constant temperature much lower than the flame temperature and thus the ethylene/air mixture has the same low temperature as it exits the burner through the plug. A peak temperature of ~1750 K is reached at 4 mm HAB and then the temperature declines with height when approaching the flame stabilizer at 21 mm HAB. The decreasing temperature with height can be explained by radiation losses and the flame stabilizer acting as a heat sink. The soot primary particle diameters presented in Figure 5.2 are mean sizes evaluated from TEM studies of soot, extracted from the flame by thermophoretic sampling, see section 3.1. The particle size is seen to increase with height due to surface growth and coagulation, as discussed in section 2.2, until about 10-12 mm HAB where a plateau is reached. Part of the explanation to this plateau could be a decreasing surface growth and coagulation as the soot is graphitized, attaining the characteristics of mature soot around 12 mm HAB, as discussed in

48

Paper IX. Furthermore, as the primary particles grow larger, added volume results in smaller increase of the diameter due to the surface growing as d_p^2. While the primary particle diameter stays essentially constant above 12 mm HAB, the aggregate size, i.e. the number of primary particles per aggregate, has been seen to increase, see Paper I. The third plot in Figure 5.2 shows the soot volume fraction as function of HAB, evaluated from laser extinction measurements at 1064 nm with the value of $E(m(\lambda))$ kept constant at 0.35, see Paper X for a detailed description of the measurements. Studying the plot, a steady increase of the soot volume fraction can be seen with increasing height in the flame as the soot formation progresses according to the description in section 2.2.
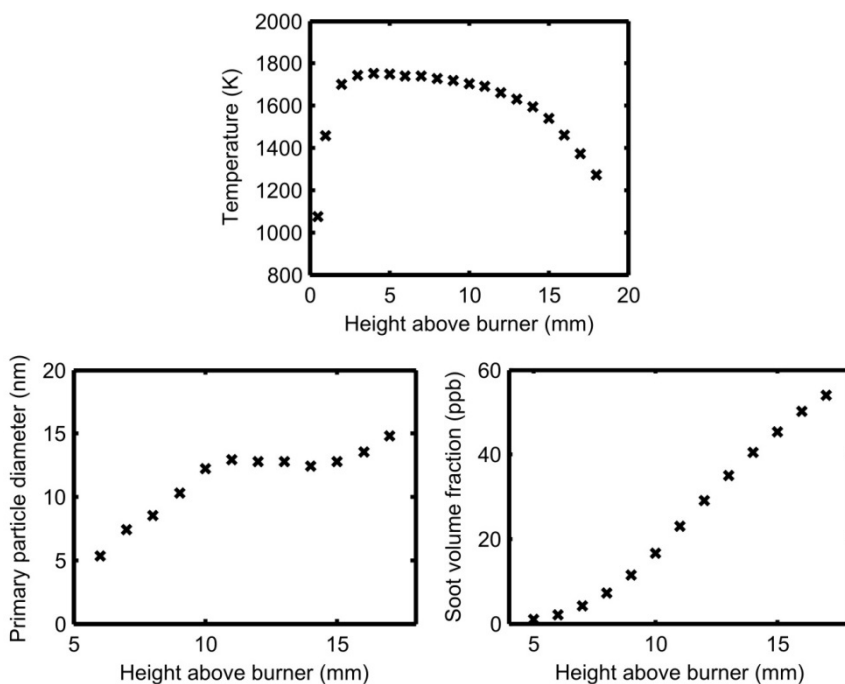
Figure 5.2
Flame temperature, mean primary particle diameter and soot volume fraction measured at different HAB in a premixed ethylene/air flame burning on a bronze plug McKenna burner at $\phi = 2.1$ with a co-flow of air.

As seen in Figure 4.2, the choice of gas for the co-flow has an impact on the flame. In Paper III the influence of the co-flow was investigated by comparison of measurements in premixed ethylene/air flames with $\phi = 2.1$ and a co-flow of either nitrogen or air. Presented in Figure 5.3 are results of measurements of the flame temperature, soot primary particle diameter and soot volume fraction along the radial direction at 10 mm HAB from the study in Paper III, together with vertical lines indicating the flame edges also seen in Figure 4.2. The largest dissimilarity seen

between the two flames is at the outer edges, i.e. a radial position of ~25 mm with the nitrogen co-flow and ~27.5 mm with the co-flow of air, see Figure 4.2. In these outer flame regions the flame with a co-flow of air has a higher temperature than in the central parts while the temperature of the flame with nitrogen co-flow decreases rapidly. The increase in temperature can be explained by the outer oxidation of unburned products occurring due to the air co-flow, while the rapid temperature decrease can be explained by cooling from the co-flow of nitrogen. Studying the central parts of the two flames, the temperature is almost the same, where the flame with air co-flow has a ~5-10 K higher average temperature, not discernable in Figure 5.3. A potential explanation to the slightly higher temperature is heating of the central parts of the flame by radiation from the warmer outer region. Also the soot size and volume fraction follow the same trends in the central regions of the flames, with slightly higher values for the flame with air co-flow. At the flame edges the lower temperature of the flame with nitrogen co-flow seems to reduce the soot formation rate, effectively leading to smaller soot particles and lower soot volume fractions, while the outer oxidation surrounding the flame with air co-flow has the opposite effect.
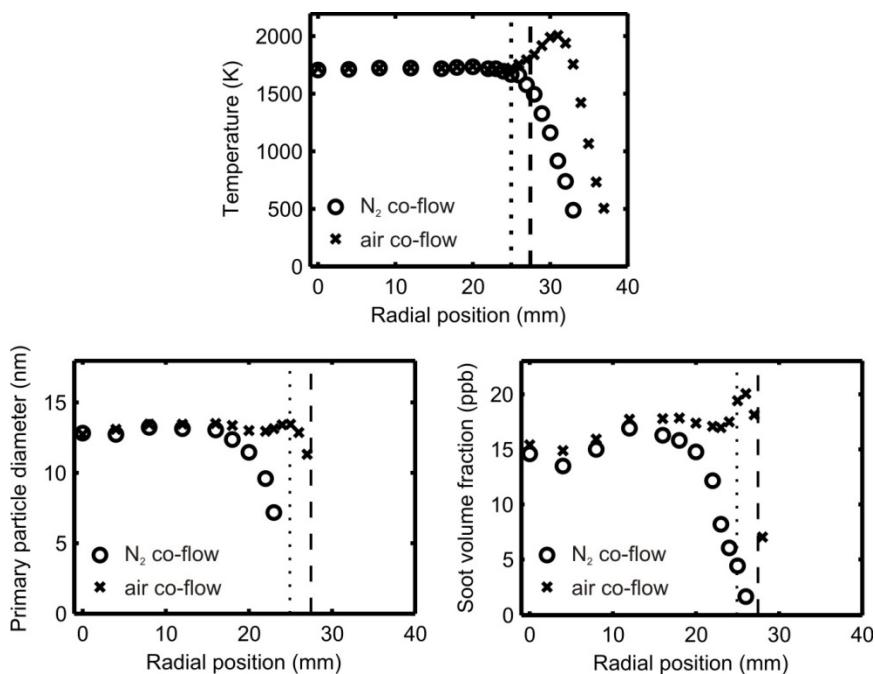
Figure 5.3
Flame temperature, primary particle diameter and soot volume fraction measured at different radial positions at HAB 10 mm in a premixed ethylene/air flame burning on a bronze plug McKenna burner at $\phi = 2.1$. Circles represent measurements in a flame with a co-flow of nitrogen and crosses correspond to a flame with a co-flow of air. The dotted line shows the position of the visual flame edge of the flame with nitrogen co-flow while the dashed line corresponds to the flame with a co-flow of air.

Considering the assumption of one-dimensionality of these flat premixed flames Figure 5.3 makes it clear that this is a somewhat erroneous assumption. While the choice of co-flow gas does not have a very large impact on the radial temperature distribution within the flame limits, there is a clear influence on the one-dimensionality of the primary particle size and soot volume fraction. The largest influence is seen at radial positions from 16 mm and outwards, especially in the case of a nitrogen co-flow, where both the soot size and volume fraction decrease towards the flame edges. This might not be a problem for point measurements or imaging measurements, but it is clearly a problem for line of sight measurements where the result is an average along the laser beam path e.g. in laser extinction. See Paper III for the complete study and discussion of the influence of co-flow gas on flat premixed flames.

Before conducting measurements in these premixed flames stabilized by a steel plate, there is a general recommendation to run the flame for about 15 minutes to heat up the stabilizer and reach a thermal equilibrium for the system before conducting any measurements [10]. In Paper III it was tested whether this actually has any influence on the flame, or more specifically on the soot generated by the flame. This was done by utilizing ELS (at 532 nm) to probe for variations of the soot during 50 minutes after ignition of the flame (at 10 mm HAB in a premixed ethylene/air flame with $\phi = 2.1$). ELS was used as probing technique due to the high sensitivity to changes of the soot particle size as the light scattering is proportional to d_p^6, see Eq. (3.13). The result is plotted in Figure 5.4 and a slight increase of the signal can be seen during the ~10 first minutes. However, since the scattering signal is not only dependent on the primary particle size, but also the aggregate size, particle number density and complex refractive index, the signal increase cannot solely be attributed to an increase of the size of the primary particles. The increase of the signal is nevertheless an indication of a change of the soot properties. Thus it is verified that the recommendation of a ~15 minute heat up time holds. However, when the same kind of measurement series over time was done with CARS, no temperature variation could be discerned.
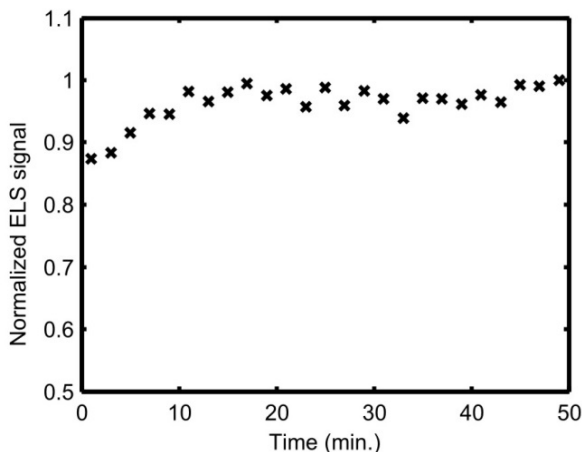
Figure 5.4
The normalized ELS signal (532 nm), plotted over time, from a premixed ethylene/air flame at $\phi = 2.1$ and HAB 10 mm burning on a bronze plug McKenna burner with a co-flow of air.

5.1.2 Optical investigations of soot properties and maturity

When conducting measurements on soot at different heights in flat premixed flames, it involves measuring on soot at different stages in the soot formation process i.e. soot at different levels of maturity. In this section the results from studies of soot properties in flat premixed flames are summarized and differences found between nascent and mature soot are discussed. The presented data originates from the studies presented in Paper I, V, VI, IX, and X.

The absorption function can be evaluated from time-resolved LII data using a numerical model for LII, following the method introduced by Snelling et al. [80], which was done as part of the studies in Paper I and IX. The evaluation routine requires a number of parameters to be known and that the measurements are made in the low-fluence regime, below the sublimation threshold of the soot, so that the sublimation (see section 3.2.4 and Eq. (3.23)) can be disregarded in the modelling. To begin with, the flame temperature and the soot particle temperature are required and these can be measured by for example rotational CARS and two-color pyrometry, respectively. The absorption rate, described by Eq. (3.19), is then adjusted in the modelling so that the modelled soot peak temperature equals the experimentally evaluated one. This is done by varying the value of the absorption function until a best fit between the temperatures is found, resulting in a value of $E(m(\lambda))$ at the laser wavelength. Studying Eq. (3.19) it can be seen that this evaluation scheme requires the laser pulse energy, laser spatial and temporal profiles and primary particle size to be known. However, by evaluating at the signal peak, the influence of the particle size on the result is minimized due to the soot particles being volume

absorbers, resulting in essentially the same peak temperatures independent of size as discussed in section 3.2.4.1. The inferred value of $E(m(\lambda))$ by this method is valid at the laser wavelength, which for the studies in this thesis is 1064 nm. Furthermore, since the inferred value is based on soot heated more than 2000 K it is an effective value for a range of soot temperatures, thus including effects taking place during the heating e.g. graphitization of the soot.

The absorption function has been evaluated at a wavelength of 1064 nm for soot at different HAB in flat premixed ethylene/air flames at both $\phi = 2.1$ and $\phi = 2.3$ in Paper IX. In Figure 5.5 the resulting values for $E(m)$ at a wavelength of 1064 nm are presented at 8, 9, 10, 12 and 14 mm HAB for both of the investigated flames. The evaluated values are lower at all heights in the $\phi = 2.1$ flame except for at 14 mm HAB, most likely due to a slower soot formation process, i.e. a lower degree of maturity at corresponding heights. Both flames display an increasing trend of the absorption function with increasing height in the flames. This can be explained by the increasing soot maturity with height in the flames, where the more mature soot at higher HAB absorb more efficiently due to the higher fraction of graphitic bonds, i.e. sp^2 bonds [7]. Apart from the studies in conjunction to this thesis, there are several other investigations where an increasing absorption efficiency with increasing soot maturity has been evaluated, see for example [81, 87, 104]. By further analyzing Figure 5.5 the increase of the evaluated values of the absorption function can be seen to almost cease above ~10-12 mm HAB, indicating that an essentially constant level of maturity is reached above these heights in the flame with an $E(m)$ value around 0.35 at a wavelength of 1064 nm. This value is in good agreement with previously reported ones, see [10, 105] and references therein.
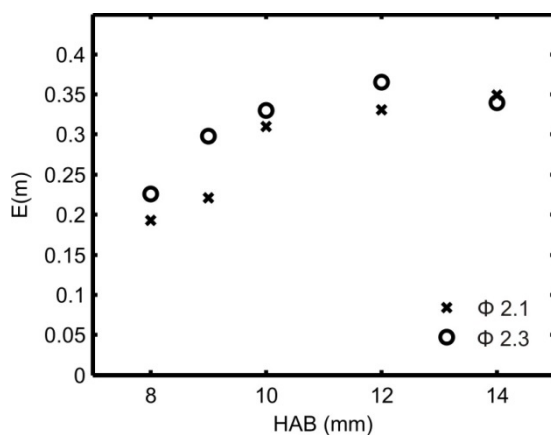

Figure 5.5
$E(m)$ at 1064 nm evaluated from LII measurements at a laser fluence of 0.14 J/cm^2 at different HAB in flat premixed ethylene/air flames at $\phi = 2.1$ and $\phi = 2.3$.

An important point to consider when evaluating $E(m(\lambda))$ from LII data using the described method is a potential change of the soot properties as a result of the rapid laser heating for example laser induced graphitization, as has been suggested to occur [87, 106, 107] and effectively increase the absorption efficiency. This could affect the inferred values of the absorption function, especially at the lower flame heights, potentially resulting in higher evaluated values. Additionally, a key assumption that is made when evaluating the absorption function using LII is that the product $\rho_s \cdot c_s$ stays constant throughout the absorption process and also for soot at different levels of maturity.

The absorption function has a wavelength dependence through the complex refractive index which is wavelength dependent, as mentioned in section 2.3 and discussed in detail in [7]. A suggested wavelength dependence of the absorption function has been presented in several studies, with significant discrepancies in some cases, see for example [10, 105, 108, 109] and references therein. Some of the differences can likely be explained by the different soot sources used, producing soot with different properties, such as the differences seen between nascent and mature soot. A varying wavelength dependence of the absorption function with soot maturity in premixed ethylene/air flames is discussed to some extent in Paper IX and X, and an attempt is made for predicting the wavelength dependence at different HAB in flat premixed ethylene/air flames. As seen in Eq. (3.5), the absorption of light by soot particles has a $\sim 1/\lambda$ dependence within the Rayleigh limit. By assuming the scattering to be negligible in the laser extinction measurements in Paper X, where extinction was measured in flat premixed ethylene/air flames at different HAB and with different laser wavelengths, the absorption was seen to deviate from the predicted $\sim 1/\lambda$ dependence at low HAB. This deviation was incorporated as a dispersion coefficient α for the wavelength dependence of the absorption using Eq. (3.5),

$$K_{abs} = \frac{\pi^2 E(m_{ref})}{\lambda^\alpha} N d_p^3,$$ (5.1)

where m_{ref} is a constant complex refractive index used in the evaluation. A wavelength dependence for $E(m(\lambda))$ can be achieved by instead interpreting α as a wavelength dependence of the absorption function as,

$$E(m(\lambda)) \propto \lambda^{1-\alpha}.$$ (5.2)

The inferred α from Paper X is plotted in Figure 5.6 as function of HAB for two flat premixed ethylene/air flames at $\phi = 2.1$ and $\phi = 2.3$. As can be seen in the figure, the dispersion coefficient seems to approach a value of 1 for heights above ~12 mm, suggesting an essentially wavelength independent absorption function. This is in quite

54

good agreement with results reported for mature soot in similar studies, see [108] and references therein. However, up to ~12 mm HAB α is seen to decrease, indicating a decreasing wavelength dependence of $E(m(\lambda))$ with increasing HAB. Similar indications have also been found in other studies, see for example [51, 110]. An important implication of these results is for soot temperature evaluation using the two-color pyrometry procedure outlined in section 3.2.3. A wavelength dependent absorption function makes the assumption $E(m(\lambda_2))/E(m(\lambda_1)) = 1$ erroneous, resulting in the evaluated temperatures at lower HAB being incorrect. However, using the results presented in Figure 5.6 together with (5.2), it is possible to correct for the wavelength dependence in the temperature evaluation. This was done for temperature evaluations of soot in Paper IX, resulting in lower temperatures than first evaluated when not accounting for a wavelength dependent absorption function.
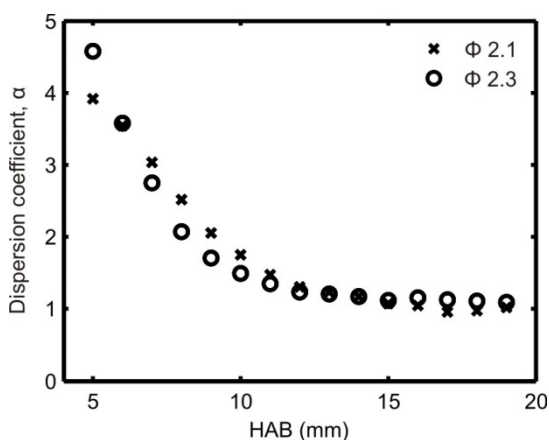

Figure 5.6
Dispersion coefficient, α, plotted as function of HAB for flat premixed ethylene/air flames at $\phi = 2.1$ and $\phi = 2.3$.

Another important soot property when conducting LII measurements is the soot sublimation threshold, defining the transition point between the low fluence and high fluence regimes, see section 3.2.4. The sublimation threshold is commonly defined at a certain laser fluence or a temperature. However, there are differences between these two measures of the sublimation threshold that are important to take into consideration. A sublimation fluence threshold is not a pure soot property, since it also depends on the laser properties, i.e. wavelength (due to the wavelength dependence of the absorption, Eq. (3.5)) and spatial and temporal profiles, and the flame temperature (the soot has to be heated from the flame temperature to the soot sublimation temperature). Furthermore, a fluence threshold also depends on the value of the absorption function, meaning that the level of soot maturity also has an influence on the fluence threshold. Accounting for these aspects, the benefit of using a laser fluence threshold is that it is simpler to measure and monitor the laser fluence

than the soot temperature. Soot sublimation thresholds at different HAB in premixed ethylene/air flames were evaluated for flames at $\phi = 2.1$ and $\phi = 2.3$ in Paper IX. This was done by using a pump-probe combination of two-color LII and ELS, where a laser at 1064 nm was used to heat the soot and two-color LII was utilized to determine the soot temperature, while ELS was used to probe for the onset of sublimation. Both the sublimation fluence threshold and temperature threshold from Paper IX are plotted in Figure 5.7 for different HAB in the two flames. The presented temperature thresholds are corrected for a wavelength dependent $E(m(\lambda))$ using the results from Figure 5.6. Uncorrected temperature thresholds are presented in the full study, see Paper IX. The threshold values, both the fluence and the temperature, are converging towards an essentially constant value above ~12-14 mm HAB. This can most likely be explained by the soot reaching a certain level of maturity above ~12 mm HAB, as also seen in the results presented in Figure 5.5 and Figure 5.6. The sublimation temperature threshold at ~3400 K for mature soot at heights above ~12 mm agrees well with previously presented results by Liu et al. [111] where a value of 3300-3400 K was found.
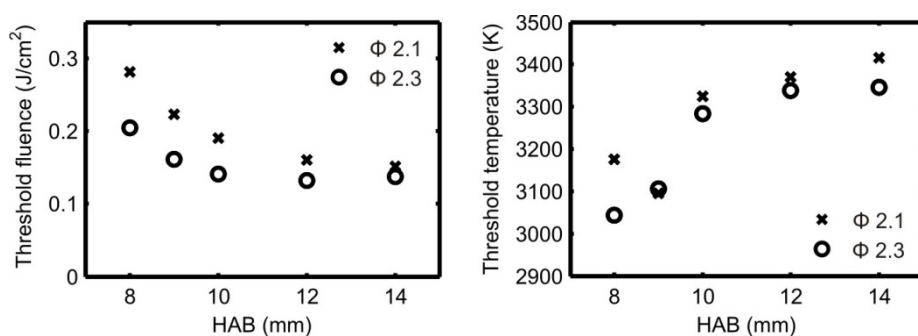
Figure 5.7
Sublimation fluence and temperature thresholds evaluated at different HAB in flat premixed ethylene/air flames burning at $\phi = 2.1$ and $\phi = 2.3$.

As the soot properties vary with soot maturity the LII signal response will inevitably also be altered. In Paper VI a detailed investigation was made of the LII signal detected from very small nascent soot particles found in low-sooting flat premixed flames using an experimental setup with high detection sensitivity. The results of this study indicate that the LII signal from the smallest detectable nascent soot particles in the studied flames do not show the same behavior with increasing laser fluence as commonly seen. The fluence curves do not display an S-shape as seen for the fluence curve presented in Figure 3.5, at least not within the fluence range where an S-shape is typically seen. Instead the LII signal was found to increase linearly with increasing laser fluence for these soot particles within the studied laser fluence range. Presented in Figure 5.8 is a comparison of fluence curves measured at 12 mm HAB in flat premixed ethylene/air flames burning at different equivalence ratios. A flame with an

equivalence ratio of 1.77 was the lowest sooting flame in which a signal could be detected with the setup used.
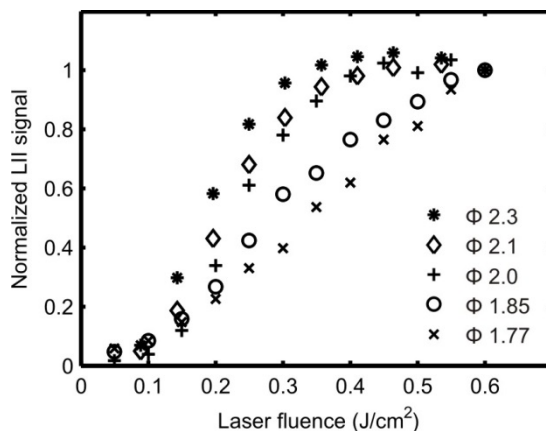

Figure 5.8
LII fluence curves, i.e. signal as function of laser fluence, for different equivalence ratios of flat premixed ethylene/air flames on a McKenna burner, measured at 12 mm HAB. The plotted results are normalized at the measurement point corresponding to the highest laser fluence, 0.6 J/cm^2.

In Figure 5.8 the fluence curves at the different equivalence ratios are seen to gradually transition from the commonly seen S-shape to a linear behavior at $\phi = 1.77$. This linear shape of the fluence curve was seen at all studied heights in the $\phi = 1.77$ flame, from 8 mm to 16 mm HAB and also in the $\phi = 1.85$ flame at heights up to 10 mm HAB. Another interesting observation in the $\phi = 1.77$ flame was that the LII signal decay time did not change with height, suggesting essentially constant particle properties throughout the flame. Thus it seems like particle nucleation takes place, but only minor soot growth i.e. surface growth and coagulation. The inevitable question that arises is if the detected signal really is thermal emission from particles or if it could be some kind of LIF signal, induced from large PAHs. The following reasoning and analysis led to the conclusion that the origin of the signal really was thermal emission, i.e. LII.

1. A laser wavelength of 1064 nm was used to heat the soot particles to avoid LIF, even from the largest PAH molecules. The longest excitation wavelength at which LIF interference has been detected is ~700 nm [61, 62]. This is further strengthened by the results from the laser extinction study in Paper X, where no absorption except for that from soot was observed at wavelengths longer than 700 nm.

2. The possibility of a LIF signal from two-photon excitation was ruled out due to a combination of weak absorption cross-sections and low concentrations of PAHs large enough to generate such a signal.

3. Planck's law, Eq. (2.7), could be fitted to measured spectra showing broad band emission at low HAB in the $\phi = 1.85$ flame. Unfortunately, the signal-to-noise ratio at $\phi = 1.77$ was not high enough to achieve any spectra for analysis.

4. Two-color LII measurements were made at 10 mm HAB in the $\phi = 1.85$ flame for laser fluences up to 1.5 J/cm², resulting in a fluence curve indicating an S-shape. Furthermore, evaluation of the two-color data resulted in evaluated temperatures approaching 4000 K for the highest fluence.

The results indicate that nascent soot particles with sizes on the order of a few nm can be detected using LII. However, their optical and physical properties likely differ substantially from those of soot at the later stages in the formation process, probably being the reason for the essentially linear relationship between signal and laser fluence observed. These results show potential for utilizing LII as a tool to study newly nucleated soot particles, of which important knowledge is lacking to accurately model the nucleation process.

5.2 Processes affecting time-resolved LII signals

The physics behind the time-resolved LII signals are complex and challenging to model due to the numerous processes taking place during the rapid laser heating and successive cooling of the soot particles. Results from the studies made in Paper II and VII, where processes affecting time-resolved LII signals were investigated, will be summarized in this section.

5.2.1 Soot aggregation

The decay time of the LII signal depends on soot primary particle size, as described in section 3.2.4, where the decay time is longer for larger primary particles due to a decreasing surface-to-volume ratio. However, it can also be reasoned that when the soot starts to form aggregates, the heat loss rate should decrease even more. This decrease would result from a shielding effect where the primary particles in the aggregate shield each other from impinging atoms and molecules, leading to a decrease of the heat conduction rate of the aggregate. A shielding effect like this has been modelled in a number of numerical investigations that all indicate an actual influence of aggregation on the temperature decay of laser heated soot particles, see for example [73, 74, 84, 112]. Experimental investigations of aggregate shielding are however scarce, and presented in Paper II is, to my knowledge, the first experimental investigation of the influence of a shielding effect on the decay time of time-resolved LII signals.

For the investigation in Paper II an in-house built soot generator resembling the commercial CAST system [113] was used for generation of the soot particles. The generator consists of two coannular tubes with a flow of propane in the center and a co-flow of air, producing a laminar diffusion flame. At a height of 55 mm above the burner surface a horizontal stream of air, at a constant flow, was used to quench the flame and thereby produce a homogenous and steady flow of soot particles. By variation of the propane and air flows, the morphology of the generated soot could be altered. A detailed description of the soot generator can be found in [114]. By a combination of TEM, SMPS and DMA-APM measurements, see section 3.1, the emitted soot could be characterized in terms of soot primary particle size and number of primary particles per aggregate. Using these techniques, three different operating conditions were found at which the primary particle sizes were practically the same while there was a significant difference between the aggregate sizes. These operating conditions were termed Case A, B and C and in Figure 5.9 the primary particle size distributions are displayed together with TEM images for each of the three cases, where Case A corresponds to the smallest aggregates and Case C to the largest.
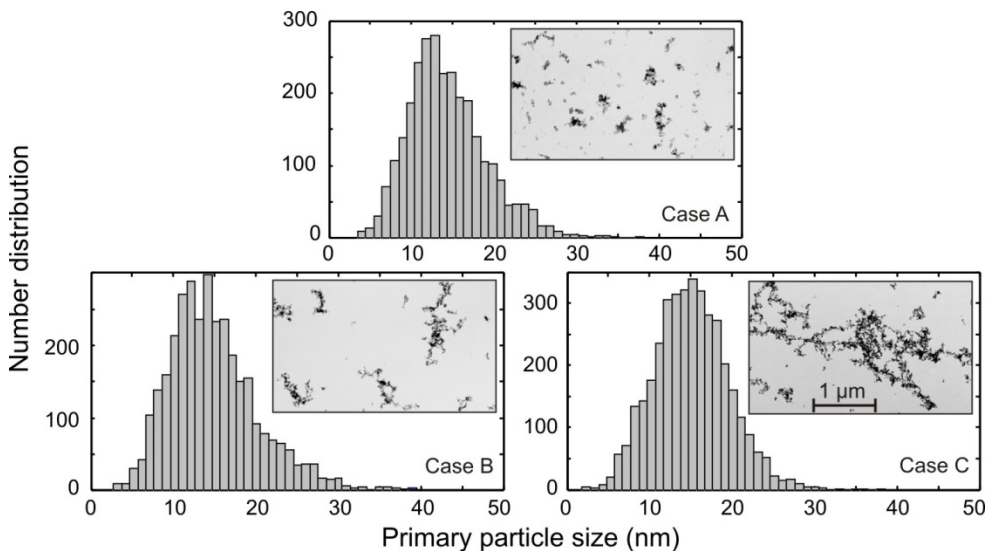
Figure 5.9
Evaluated soot primary particle size distributions presented together with TEM images for the three operating conditions used, named Case A, Case B and Case C.

Two-color LII measurements were conducted for each of the three cases using a setup similar to the one described in detail in section 4.2. For further experimental details see Paper II. The resulting time-resolved LII signals for the three cases are presented in Figure 5.10. A significant difference in decay time is seen when comparing the LII signals from the three cases. Furthermore it can be noted that the signal with longest decay time corresponds to Case C and the signal with shortest decay time corresponds

to Case A. This is in agreement with the aggregate shielding theory [73, 84] and previously mentioned modelling results, predicting that larger soot aggregates result in longer LII signals.

Figure 5.10
A comparison of experimentally measured time-resolved LII signals for three separate operating conditions of the soot generator, Case A, B and C.

In addition to the two-color LII measurements and visual comparison of the time-resolved curves presented in Figure 5.10 our numerical model for LII was used to further analyze the data, with and without using the aggregation mechanism developed 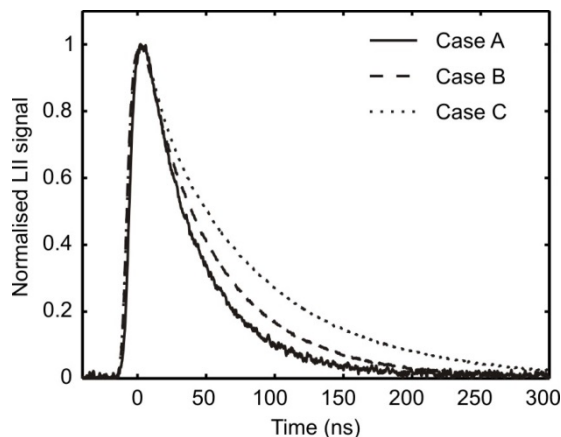by Liu et al. [84]. Evaluation of primary particle diameters from the experimental curves using the LII model without accounting for aggregation resulted in monodisperse equivalent sizes of 19, 26 and 36 nm for Case A, B and C, respectively. A clear disagreement is seen when comparing the diameters evaluated using the model to the ones evaluated from the TEM data, presented in Figure 5.9. Utilizing the aggregation mechanism and the primary particle sizes in Figure 5.9, the model was used to simulate LII signals for the three cases. While the same trend was achieved, with longest signal for Case C and shortest signal for Case A, the same quantitative difference of decay times could not be reached for the modelled signals. It could however not be clarified whether this was purely due to the model failing to reproduce the influence of aggregation on the signal decay, or if the differences seen between the decay times in Figure 5.10 are a combined result of aggregation and differing soot properties between the three cases (e.g. thermal accommodation coefficient). Nevertheless, the results strongly suggest that at least part of the explanation to the observed difference between decay times lies in an increasing shielding effect with increasing level of aggregation.

5.2.2 Local gas heating

When an LII measurement is performed, where the soot is rapidly heated to temperatures up to ~4000 K and then cools down to the ambient temperature, it can be argued that the heat carried away from the soot should be deposited in the ambient gas (except for the fraction of heat lost by radiation). Depending on the soot volume fraction and how fast the heat diffusion is, this could possibly lead to a noticeable local gas heating effect in the measurement volume i.e. the volume affected by the laser light. An effect like this was discussed by Eckbreth already in 1977 [115], who made theoretical estimates of the heat diffusion rate from laser heated soot. The conclusion was that a gas heating effect due to heat conduction from laser heated soot should be seen on a time scale of ~10-100 ns for typical soot sizes presented in this thesis. Another study on the same subject was made by Snelling et al. [116] who, in addition to theoretical predictions, also made an experimental investigation using two-color pyrometry. The results indicated a significant local gas heating in an ethylene/air diffusion flame burning on a Gülder burner, described in section 4.1.2.

In Paper VII a combination of two-color LII and rotational CARS was utilized to experimentally investigate the gas heating effect induced by laser heated soot in the same diffusion flame as used in [116] and described in section 4.1.2, with a soot volume fraction of ~4.0 ppm at the measurement position. The gas temperature increase evaluated from CARS measurements is plotted in Figure 5.11 as a function of delay time between the heating laser pulse (1064 nm) and the CARS probe pulse for two different laser fluences of the heating laser. A laser fluence of 0.14 J/cm^2 was chosen to get as high gas heating effect as possible with only minor sublimation of the soot occurring, while a laser fluence of 0.40 J/cm^2 was chosen to have a measurement case where major sublimation is present.
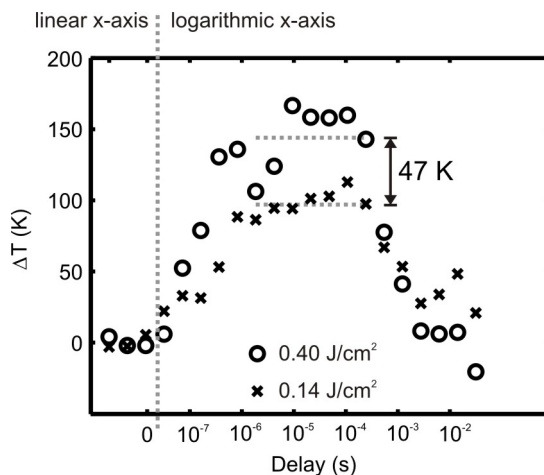
Figure 5.11
Increase of the gas temperature as a result of heat transfer from soot particles heated using a laser at 1064 nm and laser fluences of 0.40 and 0.14 J/cm², as indicated in the figure. The temperature is evaluated from rotational CARS measurements at different delay times to the heating laser pulse. The vertical dotted line indicates where the x-axis changes from linear scale to logarithmic and the horizontal dotted lines indicate the mean values at the plateau regions of the two data sets.

Studying Figure 5.11, the gas temperature is seen to increase some 10´s of K already within the first 100 ns, reaching a plateau at delay times on the order of µs i.e. the soot particles and the gas are at temperature equilibrium. The temperature is seen to decrease back to the original flame temperature at times from ~0.1 ms to a few ms which is interpreted as a combination of thermal diffusion and the heated gas volume being swept away by the vertical gas flow in the flame. Additionally, two dotted horizontal lines are seen, designating the mean temperature increase in the estimated plateau region (the region covered by the dotted lines). Thus, the evaluated temperature increase using a heating laser fluence of 0.14 J/cm² is ~50 K lower than when using a heating laser fluence of 0.40 J/cm², as indicated in Figure 5.11. A higher temperature increase at a fluence of 0.40 J/cm² (inducing major sublimation) means that also part of the energy lost by sublimation from the soot is deposited in the surrounding gas.

To investigate how the local gas heating changes with increasing laser fluence, a measurement series was made where the delay between the heating laser and the CARS probe laser was kept constant at 10 µs, well within the plateau region seen in Figure 5.11, while the heating laser fluence was varied. The results of this measurement series can be seen in Figure 5.12, where a steady increase of the gas heating is seen as a function of laser fluence throughout the studied fluence range.
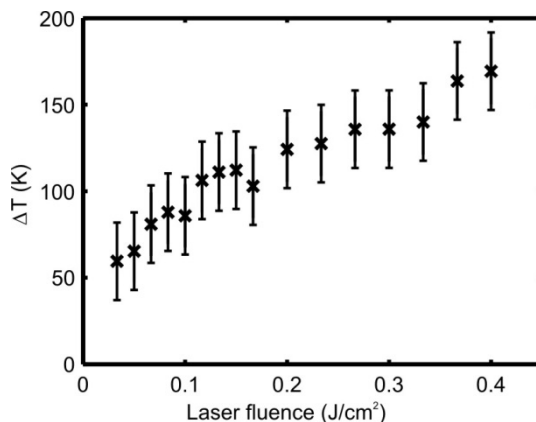
Figure 5.12
Temperature increase of the gas due to heat transfer from laser heated soot particles plotted as function of heating laser fluence. Temperatures are evaluated using rotational CARS and the error bars represent an estimated uncertainty from a series of measurements.

The consequences of gas heating for LII are mainly of importance when evaluating time-resolved LII signals since the gas heating is taking place simultaneously with the decay of the LII signal i.e. as the soot cools down after the heating laser pulse has passed. Since the effective gas heating is gradual, so is the impact on the LII signal. Hence, if not taking the gas heating into account, a lower heat conduction rate is to be expected due to the increase of ambient gas temperature. The effect of this on time-resolved LII signals is a somewhat longer decay time than predicted. Thus particle sizes evaluated from time-resolved LII signals will be slightly over predicted if gas heating is not considered.

5.3 LII applied for measurements of soot volume fractions

In practical combustion devices LII is commonly applied for 2D measurements of soot volume fractions, f_v, as described in section 3.2.4. In Paper IV and VIII, LII was used for 2D mapping of the soot volume fraction in partially premixed vaporized liquid fuel flames and diluted unstrained flat CH_4/O_2 diffusion flames, respectively.

In Figure 5.13 some of the results from measurements in a partially premixed flame burning vaporized n-heptane (C_7H_{16}) at $\phi = 3.7$ are displayed. The images were collected by an ICCD camera, for experimental details see Paper IV and for a detailed description of the burner see [117]. Both 266 nm and 1064 nm were used as laser wavelengths to heat the soot. By using a laser wavelength of 266 nm both laser-induced fluorescence (LIF) from PAH and LII from soot were acquired at the same time. The prompt signal resulting from the 266 nm laser is displayed in pane a) in

Figure 5.13, showing the overlapping LIF and LII signals. In pane b) the signal induced by the 266 nm laser is detected using a gate delayed by 50 ns to the laser pulse, thus only detecting LII due to the much shorter decay time of LIF compared to LII. While the signals in a) and b) are only qualitative, pane c) displays the soot volume fraction evaluated from LII measurements using a laser wavelength of 1064 nm (thus avoiding PAH LIF). Comparing the three panes to each other it becomes clear that the top part (around 15 mm HAB) of the signal from prompt detection at 266 nm excitation originates from LII, while the signal below ~13 mm HAB can be related to LIF from PAH. Another interesting observation that can be made when following the vertical center line is that as the PAH signal decreases with height, after reaching a peak around 12 mm HAB, the LII signal increases. This can be interpreted as the PAH molecules, i.e. soot precursors, being consumed when the soot particles are formed. Measurements were also made using n-decane ($C_{10}H_{22}$) as fuel, resulting in the same trends, but with higher soot volume fractions. At $\phi = 3.7$ the n-decane flame produced about a factor 1.3 higher peak soot volume fraction than the n-heptane flame. More details and results from the measurements in vaporized n-heptane and n-decane flames are found in Paper IV.
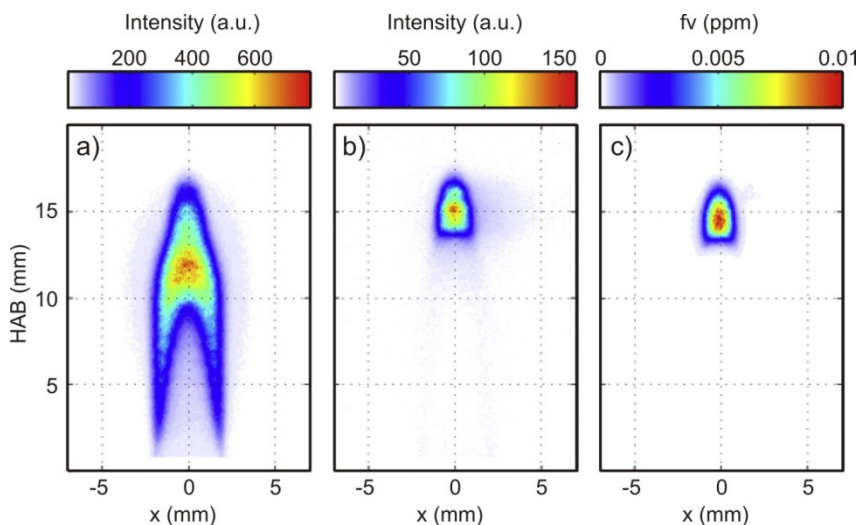
Figure 5.13
2D laser-induced signals from a partially premixed vaporized n-heptane flame burning at $\phi = 3.7$. Pane a) displays the overlapping signals of LII and PAH LIF resulting from prompt detection using 266 nm laser excitation, b) shows the signal when delaying the gate in a) by 50 ns, thus only collecting part of the LII signal decay and c) shows the evaluated soot volume fraction using 1064 nm excitation.

In Paper VIII diluted unstrained flat CH_4/O_2 diffusion flames were characterized in terms of soot volume fraction distributions by 2D LII measurements using 1064 nm laser light. While the supplied oxidant consisted of 100% O_2 the fuel gas flow was diluted with CO_2 to achieve different volume fractions of CH_4, effectively varying the

mixture strength while keeping the flow speed constant. A picture of one of the sooting flames is displayed in Figure 5.14 burning at $\phi = 2.18$ (here defined as the mixture strength of the provided CH_4 and O_2), where the sooting region can be recognized as the brightly yellow layer of a few mm thickness. A detailed description of the burner is available in [118].
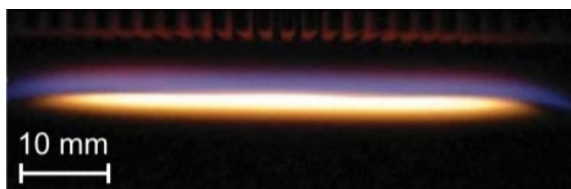
Figure 5.14
A photograph of a sooting flat diffusion flame burning at $\phi = 2.18$.

A wide range of flames with different mixture strengths and gas flows were investigated, of which only some are presented in Paper VIII. The vertical soot volume fraction distribution for seven flames with different volume fractions of CH_4 in the fuel gas flow are presented in Figure 5.15. The shape of the spatial soot distribution is similar for all of the mixture strengths, with increasing volume fraction and width of the soot layer for increasing volume fractions of CH_4. The soot volume fraction is seen to gradually increase from lower to higher heights i.e. from lower to higher temperatures as the fuel is pyrolyzed and soot is formed. A peak f_v is reached at a certain height, above which a rapid decrease can be seen due to oxidation of the soot. This behavior is representative for all of the investigated flames.
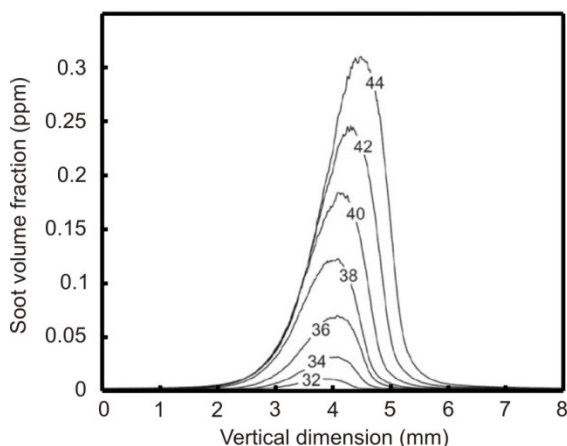
Figure 5.15
Soot volume fraction distributions along the vertical direction in seven different unstrained flat CH_4/O_2 diffusion flames, evaluated from 2D LII measurements. The CH_4 volume fraction ranges from 32% up to 44%, as indicated in the figure.

As discussed in 3.2.4, the largest uncertainties when quantitatively evaluating soot volume fractions using LII stem from the calibration procedure and the choice of $E(m)$, assuming a laser wavelength of 1064 nm is used so PAH LIF interference of the signal can be neglected. In both Paper IV and VIII calibration was performed in flat premixed ethylene/air flames in which the soot volume fraction was originally evaluated using laser extinction. Thus the uncertainty from the extinction technique propagates to the evaluated soot volume fractions using LII. Most notable is the uncertainty related to $E(m)$, for which an absolute value is required to determine f_v by laser extinction. This has been discussed in section 2.3 (soot properties), 3.2.1 (laser extinction) and 3.2.4.3 (LII). The soot volume fraction in the premixed ethylene/air flames used for calibration in Paper IV and VIII was evaluated using $m = 1.56 - 0.46i$ from [19], i.e. $E(m) = 0.217$. Whether this is a suitable value or not can certainly be discussed, and recent studies actually indicate that a higher value of $E(m)$ might be more appropriate to use. See for example Paper IX where $E(m)$ was evaluated to ~0.35 for HAB from ~12 mm and up in premixed ethylene/air flames at $\phi = 2.1$ and $\phi = 2.3$.

6 Summary and outlook

The conducted work displays a variety of ways in which LII can be applied for measurements of soot properties, both on its own and in combination with other diagnostic techniques. The main part of the work has been done with an aim to improve the knowledge about soot particle properties and how these affect the LII signal, knowledge that is crucial for conducting accurate LII measurements and evaluations. Additionally, LII has been used as a tool to characterize different laboratory flames in terms of soot properties.

Maturity of soot and differences between nascent and mature soot have been investigated and discussed to some extent in Papers I, V, VI, IX and X, where the soot formation was followed as a function of HAB in flat premixed ethylene/air flames. In Paper VI the LII signal response of newly nucleated nascent soot particles was studied in low-sooting premixed flames and the results revealed significant differences in comparison to the signals commonly seen. Even though the results are challenging to interpret, they show potential for LII as a diagnostic technique for investigations of these newly nucleated soot particles. The thermal accommodation coefficient of soot and its evolution with soot maturity was discussed in Paper I, where the results indicate a decreasing trend with HAB. The absorption function and its variation with soot maturity and wavelength were discussed and investigated in Papers I, V, IX and X. Results from these studies suggest an increasing $E(m)$ with height, reaching a value of ~0.35 for mature soot. While $E(m)$ seems to be almost wavelength independent for mature soot, the results suggest that $E(m)$ decreases with wavelength for nascent soot particles. Using a combination of LII and ELS, the sublimation threshold and its variation with soot maturity were investigated in Papers V and IX, where the sublimation threshold temperature was found to increase slightly with soot maturity and reach an essentially constant value around 3400 K for mature soot.

The behavior of time-resolved LII signals and processes affecting these were investigated in Paper II and VII. In Paper II LII was utilized together with SMPS and DMA-APM to investigate the influence of soot particle aggregation on time-resolved LII signals. The results show that aggregation of soot particles leads to longer LII signals, likely due to a shielding effect that decreases the heat conduction rate and thus results in longer decay times of the LII signals with increasing levels of aggregation. The study in Paper VII was aimed at investigating a potential gas heating effect as laser heated soot cools down, resulting in an increase of the surrounding gas temperature. By combining LII with rotational CARS for temperature measurements,

the gas temperature was found to increase ~100 K in a flame with 4 ppm of soot when heating the soot by ~2000 K.

LII was also applied for characterization of laboratory flames. In Paper III the premixed ethylene/air flame standardized within the LII community was investigated at $\phi = 2.1$ for co-flows of air and nitrogen. The results show uneven soot distributions along the radial axis, differing with choice of co-flow gas. Thus the assumption of one-dimensionality is somewhat violated and also depends on the choice of co-flow gas. Additionally, flames burning vaporized n-heptane and n-decane were characterized in Paper IV in terms of soot volume fraction distributions and in Paper VIII soot volume fraction distributions were measured in diluted unstrained flat CH_4/O_2 diffusion flames.

The main contributions from this work to the LII community are the results concerning differences of soot properties between nascent and mature soot, and knowledge of $E(m)$ and its variation with soot maturity and wavelength. These are important subjects for improving the LII models and thereby also the accuracy of the LII technique. Furthermore, this is knowledge that can be used within other fields of research as well. It is also interesting for combustion and climate modellers for improving the knowledge about soot particles, how they evolve with time and the impact of soot emissions on the climate.

Of large importance for the development and improvement of the LII technique is the international workshop on LII taking place every 2nd year. The first meeting was held in Duisburg, Germany 2005 and the sixth one was held on the island of Ven in Sweden 2014. At these meetings the recent findings on LII are discussed in a collaborative effort to solve arisen questions and obstacles. Two good examples of the outcomes of these collaborative efforts are [10, 119], where the results of different research groups within the LII community are compared and discussed. It is important for future development and progress of the LII technique that these meetings continue, so the most recent trends and questions can be debated in a familiar environment. The next LII workshop is scheduled for 2016 and will be hosted by Sandia National Laboratories in USA.

Another workshop that has been initiated is the international sooting flame (ISF) workshop where modelers are brought together with experimentalists to compare their results. This workshop is held every 2nd year in conjunction with the International Symposium on Combustion. The first workshop took place in Warsaw, Poland, 2012 and the second one was held in conjunction with the symposium in San Francisco, USA, 2014. The aim of the workshop is to designate target flames for both modelling and experimental measurements, and compare the results. This kind of validation is crucial for confirming that the results are reliable as well as for improving the knowledge on soot formation and soot properties. Cross-disciplinary collaborations like this are very useful for further developing the LII technique by

finding out what knowledge other fields are lacking and also by filling knowledge gaps within the LII field of research.

7 Acknowledgements

I would like to start by expressing my gratitude to the head of the division of Combustion Physics, **Marcus Aldén**, for providing a great place to work at with a friendly and familiar environment. I have had five amazing years at the division and made many good friends. This would not have been possible without your hard work Marcus, resulting in what is now the division of Combustion Physics.

Five years ago, when I started at the division, I had the good fortune to get two great supervisors, **Per-Erik Bengtsson** and **Henrik Bladh**. I clearly remember my arrival in Lund, when you were tidying up the small apartment that became my home for the first few months. It was great to feel welcome in a place where I essentially knew no one. You both have been more supportive and helpful than I could ever ask for, and for that I am very grateful. To me you are not only my supervisors and mentors, I also consider you as two good friends. Thank you for making these past years so delightful and educative!

I would also like to thank you **Jonathan Johnsson**, both for your help with the research during the years we worked together in our small research group and for other times we spent together. We had a lot of fun in China, at least until we tried KFC in Shanghai… and yeah, thank you for bringing Imodium, or was it you? I have a hard time remembering since I had other urgent matters demanding my attention…

Furthermore, I would like to thank our latest recruits to the LII research group, **Johan Simonsson** and **Sandra Török**. Thank you for relieving me of some of my duties during the writing of this thesis.

There are also many others at the division of Combustion Physics to whom I am very thankful. **Rikard Wellander**, thank you for teaching me the ABCs of what to be aware of when buying a house, how to take the house apart when you bought it and finally how to rebuild the house once you took it apart. However, most of all I would like to thank you for being an amazing and very supportive friend. **Malin Jonsson**, I would also like to thank you for being the best of friends and for all of your support during these years. I am very happy to have got to know you; together we have travelled the world and we have had loads of fun – let us continue that way! **Moah Christensen**, thank you! You are one of the oddest and funniest persons I have had the privilege to meet and you are a wonderful and caring friend as well. Without you I would not know the true meaning of getting "scared shitless", let us continue finding those greatest of horror movies, just maybe not as scary as "The Conjuring".

Emil Nordström, it is you I have to thank for the genius, yet utterly stupid idea to go through with completing "A Swedish Classic". This was both far more painful and fun than I ever thought it would be. I would also like to thank you for being a good friend during these years! To all you others I have learnt to know and befriended at the division, **Jesper Borggren, Johan Simonsson, Joakim Rosell, Linda Vallenhag, Edouard Berrocal, Elias Kristensson, Fahed Abou Nada** just to mention a few of you, thank you for your support and friendship. Thank all of you guys for making the "fika"-breaks so fun and for making the division of Combustion Physics such a great place to work at!

To **Johan** and **Sandra Vindelstam,** thank you for being two wonderful friends and for your support and kindness during these years. This journey would have been a lot harder without you two!

And **Emil Jonze**, you have always been an amazing and caring friend. I feel it is too challenging a task to summarize your significance for me since we met ten years ago in Umeå. Let me just say that I love you and leave it at that!

To **my family**, thank you so much for your support throughout my life. This would not have been even remotely possible without you. You have my everlasting gratitude and love!

Lastly, **Anna Svensson**, thank you my love for your support and for always believing in me. Without you it would have been much harder to write this thesis. Thank you for acting as dishwasher, cook and cleaner during these last months. You did such a great job that I feel we might as well keep it this way!

Yet again, thank you all! Without you this work would not only have been impossible, but also dull, boring, and ultimately, completely pointless.

8 References

1. IEA, *Key World Energy Statistics*. 2014. p. 1-82.
2. IPCC, *Summary for Policymakers*, in *Climate Change 2013: The Physical Science Basis. Contribution of Working Group I to the Fifth Assessment Report of the Intergovernmental Panel on Climate Change*, T.F. Stocker, D. Qin, G.-K. Plattner, M. Tignor, S.K. Allen, J. Boschung, A. Nauels, Y. Xia, V. Bex, and P.M. Midgley, Editors. 2013, Cambridge University Press: Cambridge, United Kingdom and New York, NY, USA.
3. T.C. Bond, S.J. Doherty, D.W. Fahey, P.M. Forster, T. Berntsen, B.J. DeAngelo, M.G. Flanner, S. Ghan, B. Kärcher, D. Koch, S. Kinne, Y. Kondo, P.K. Quinn, M.C. Sarofim, M.G. Schultz, M. Schulz, C. Venkataraman, H. Zhang, S. Zhang, N. Bellouin, S.K. Guttikunda, P.K. Hopke, M.Z. Jacobson, J.W. Kaiser, Z. Klimont, U. Lohmann, J.P. Schwarz, D. Shindell, T. Storelvmo, S.G. Warren, and C.S. Zender, *Bounding the role of black carbon in the climate system: A scientific assessment.* Journal of Geophysical Research: Atmospheres, 2013. **118**(11): p. 5380-5552.
4. I.M. Kennedy, *The health effects of combustion-generated aerosols.* Proceedings of the Combustion Institute, 2007. **31**(2): p. 2757-2770.
5. E.J. Highwood and R.P. Kinnersley, *When smoke gets in our eyes: The multiple impacts of atmospheric black carbon on climate, air quality and health.* Environment International, 2006. **32**(4): p. 560-566.
6. CCAC, *Climate and Clead Air Coalition: Annual Report*. 2014. p. 1-44.
7. T.C. Bond and R.W. Bergstrom, *Light Absorption by Carbonaceous Particles: An Investigative Review.* Aerosol Science and Technology, 2006. **40**(1): p. 27 - 67.
8. H. Wang, *Formation of nascent soot and other condensed-phase materials in flames.* Proceedings of the Combustion Institute, 2011. **33**: p. 41-67.
9. R.J. Santoro and C.R. Shaddix, *Laser-Induced Incandescence*, in *Applied Combustion Diagnostics*. 2002, Taylor and Francis: New York. p. 252-286.
10. C. Schulz, B.F. Kock, M. Hofmann, H. Michelsen, S. Will, B. Bougie, R. Suntz, and G. Smallwood, *Laser-induced incandescence: recent trends and current questions.* Applied Physics B, 2006. **83**(3): p. 333-354.
11. J.F. Griffiths and J.A. Barnard, *Flame and Combustion, 3rd Edition*. 1995, London: Blackie Academic & Professional.
12. S.P. Kearney and F. Pierce, *Evidence of soot superaggregates in a turbulent pool fire.* Combustion and Flame, 2012. **159**(10): p. 3191-3198.
13. C.M. Sorensen, *Light scattering by fractal aggregates: A review.* Aerosol Science and Technology, 2001. **35**(2): p. 648-687.
14. A. D'Anna, *Combustion-formed nanoparticles.* Proceedings of the Combustion Institute, 2009. **32**(1): p. 593-613.

15. S. De Iuliis, S. Maffi, F. Cignoli, and G. Zizak, *Three-angle scattering/extinction versus TEM measurements on soot in premixed ethylene/air flame.* Applied Physics B, 2011. **102**(4): p. 891-903.

16. A.D. Abid, E.D. Tolmachoff, D.J. Phares, H. Wang, Y. Liu, and A. Laskin, *Size distribution and morphology of nascent soot in premixed ethylene flames with and without benzene doping.* Proceedings of the Combustion Institute, 2009. **32**(1): p. 681-688.

17. A.D. Abid, N. Heinz, E.D. Tolmachoff, D.J. Phares, C.S. Campbell, and H. Wang, *On evolution of particle size distribution functions of incipient soot in premixed ethylene-oxygen-argon flames.* Combustion and Flame, 2008. **154**(4): p. 775-788.

18. M. Schenk, S. Lieb, H. Vieker, A. Beyer, A. Gölzhäuser, H. Wang, and K. Kohse-Höinghaus, *Morphology of nascent soot in ethylene flames.* Proceedings of the Combustion Institute, 2014(0).

19. W.H. Dalzell and A.F. Sarofim, *Optical constants of soot and their application to heat flux calculations.* Journal of Heat Transfer, 1969. **91**: p. 100-104.

20. K.H. Homann and H.G. Wagner, *Some new aspects of the mechanism of carbon formation in premixed flames.* Symposium (International) on Combustion, 1967. **11**: p. 371-379.

21. A. D'Alessio, A. Di Lorenzo, A.F. Sarofim, F. Beretta, S. Masi, and C. Venitozzi, *Soot formation in methane-oxygen flames.* Symposium (International) on Combustion, 1975. **15**(1): p. 1427-1438.

22. M. Alfè, B. Apicella, R. Barbella, J.N. Rouzaud, A. Tregrossi, and A. Ciajolo, *Structure-property relationship in nanostructures of young and mature soot in premixed flames.* Proceedings of the Combustion Institute, 2009. **32**(1): p. 697-704.

23. A. Oberlin, *Carbonization and graphitization.* Carbon, 1984. **22**(6): p. 521-541.

24. R.L. Vander Wal, *A TEM methodology for the study of soot particle structure.* Combustion Science and Technology, 1997. **126**(1-6): p. 333-357.

25. H.X. Chen and R.A. Dobbins, *Crystallogenesis of Particles Formed in Hydrocarbon Combustion.* Combustion Science and Technology, 2000. **159**(1): p. 109-128.

26. P.D. Teini, D.M.A. Karwat, and A. Atreya, *Observations of nascent soot: Molecular deposition and particle morphology.* Combustion and Flame, 2011. **158**(10): p. 2045-2055.

27. I.M. Kennedy, *Models of soot formation and oxidation.* Progress in Energy and Combustion Science, 1997. **23**(2): p. 95-132.

28. H. Bockhorn, *Soot formation in combustion: mechanisms and models.* 1994, Berlin: Springer-Verlag.

29. C.K. Law, *Combustion Physics.* 2006, Cambridge: Cambridge University Press.

30. J. Mullins and A. Williams, *The optical properties of soot: a comparison between experimental and theoretical values.* Fuel, 1987. **66**(2): p. 277-280.

31. K. Park, D.B. Kittelson, M.R. Zachariah, and P.H. McMurry, *Measurement of inherent material density of nanoparticle agglomerates.* Journal of Nanoparticle Research, 2004. **6**(2-3): p. 267-272.

32. H.A. Michelsen, *Understanding and predicting the temporal response of laser-induced incandescence from carbonaceous particles.* Journal of Chemical Physics, 2003. **118**(15): p. 7012-7045.

33. R.A. Dobbins, *Soot inception temperature and the carbonization rate of precursor particles.* Combustion and Flame, 2002. **130**(3): p. 204-214.

34. T.S. Totton, D. Chakrabarti, A.J. Misquitta, M. Sander, D.J. Wales, and M. Kraft, *Modelling the internal structure of nascent soot particles.* Combustion and Flame, 2010. **157**(5): p. 909-914.

35. K.C. Smyth and C.R. Shaddix, *The elusive history of m=1.57-0.56i for the refractive index of soot.* Combustion and Flame, 1996. **107**(3): p. 314-320.

36. T.L. Farias, Ü.Ö. Köylü, and M.G. Carvalho, *Range of validity of the Rayleigh-Debye-Gans theory for optics of fractal aggregates.* Applied Optics, 1996. **35**: p. 6560-6567.

37. C.F. Bohren and D.R. Huffman, *Absorption and scattering of light by small particles.* 1983, New York: Wiley.

38. F. Liu and G.J. Smallwood, *Effect of aggregation on the absorption cross-section of fractal soot aggregates and its impact on LII modelling.* Journal of Quantitative Spectroscopy and Radiative Transfer, 2010. **111**(2): p. 302-308.

39. W.C. Hinds, *Aerosol technology : properties, behavior, and measurement of airborne particles.* 2nd ed. 1999, New York: Wiley.

40. E.O. Knutson and K.T. Whitby, *Accurate measurement of aerosol electric mobility moments.* Journal of Aerosol Science, 1975. **6**: p. 453-60.

41. K. Ehara, C. Hagwood, and K.J. Coakley, *Novel method to classify aerosol particles according to their mass-to-charge ratio—Aerosol particle mass analyser.* Journal of Aerosol Science, 1996. **27**(2): p. 217-234.

42. R.P. Bambha, M.A. Dansson, P.E. Schrader, and H.A. Michelsen, *Effects of volatile coatings and coating removal mechanisms on the morphology of graphitic soot.* Carbon, 2013. **61**(0): p. 80-96.

43. R.L. Vander Wal, A. Yezerets, N.W. Currier, D.H. Kim, and C.M. Wang, *HRTEM Study of diesel soot collected from diesel particulate filters.* Carbon, 2007. **45**(1): p. 70-77.

44. D.B. Williams and C.B. Carter, *Transmission Electron Microscopy: A Textbook for Materials Science.* 2009, New York, NY: Springer.

45. A.C. Barone, A. D'Alessio, and A. D'Anna, *Morphological characterization of the early process of soot formation by atomic force microscopy.* Combustion and Flame, 2003. **132**(1-2): p. 181-187.

46. V. Krüger, C. Wahl, R. Hadef, K.P. Geigle, W. Stricker, and M. Aigner, *Comparison of laser-induced incandescence method with scanning mobility particle sizer technique: The influence of probe sampling and laser heating on soot particle size distribution.* Measurement Science & Technology, 2005. **16**(7): p. 1477-1486.

47. J. Hult, A. Omrane, J. Nygren, C.F. Kaminski, B. Axelsson, R. Collin, P.-E. Bengtsson, and M. Aldén, *Quantitative three-dimensional imaging of soot volume fraction in turbulent non-premixed flames.* Experiments in Fluids, 2002. **33**(2): p. 265-269.

48. R. Wellander, M. Richter, and M. Aldén, *Time resolved, 3D imaging (4D) of two phase flow at a repetition rate of 1 kHz.* Optics Express, 2011. **19**(22): p. 21508-21514.

49. S. De Iuliis, F. Cignoli, S. Benecchi, and G. Zizak, *Determination of soot parameters by a two-angle scattering-extinction technique in an ethylene diffusion flame.* Applied Optics, 1998. **37**(33): p. 7865-7874.

50. S.S. Iyer, T.A. Litzinger, S.Y. Lee, and R.J. Santoro, *Determination of soot scattering coefficient from extinction and three-angle scattering in a laminar diffusion flame.* Combustion and Flame, 2007. **149**(1-2): p. 206-216.

51. F. Migliorini, K. Thomson, and G. Smallwood, *Investigation of optical properties of aging soot.* Applied Physics B, 2011. **104**(2): p. 273-283.

52. K. Thomson, K. Geigle, M. Köhler, G. Smallwood, and D. Snelling, *Optical properties of pulsed laser heated soot.* Applied Physics B, 2011. **104**(2): p. 307-319.

53. C.J. Dasch, *Continuous-wave probe laser investigation of laser vaporization of small soot particles in a flame.* Applied Optics, 1984. **23**: p. 2209-2215.

54. B.M. Vaglieco, F. Beretta, and A. D'Alessio, *In situ evaluation of the soot refractive index in the UV-visible from the measurement of the scattering and extinction coefficients in rich flames.* Combustion and Flame, 1990. **79**(3–4): p. 259-271.

55. R.A. Dobbins, R.J. Santoro, and H.G. Semerjian, *Interpretation of optical measurements of soot in flames.* Progress in Astronautics and Aeronautics, 1984. **92**: p. 208-237.

56. J. Zerbs, K. Geigle, O. Lammel, J. Hader, R. Stirn, R. Hadef, and W. Meier, *The influence of wavelength in extinction measurements and beam steering in laser-induced incandescence measurements in sooting flames.* Applied Physics B, 2009. **96**(4): p. 683-694.

57. B. Axelsson, R. Collin, and P.-E. Bengtsson, *Laser-induced incandescence for soot particle size measurements in premixed flat flames.* Applied Optics, 2000. **39**(21): p. 3683-3690.

58. R. Wellander, E. Berrocal, E. Kristensson, M. Richter, and M. Aldén, *Three-dimensional measurement of the local extinction coefficient in a dense spray.* Measurement Science and Technology, 2011. **22**(12): p. 125303.

59. E. Kristensson, E. Berrocal, and M. Aldén, *Quantitative 3D imaging of scattering media using structured illumination and computed tomography.* Optics Express, 2012. **20**(13): p. 14437-14450.

60. R.J. Santoro, H.G. Semerjian, and R.A. Dobbins, *Soot particle measurements in diffusion flames.* Combustion and Flame, 1983. **51**: p. 203-218.

61. S. Bejaoui, X. Mercier, P. Desgroux, and E. Therssen, *Laser induced fluorescence spectroscopy of aromatic species produced in atmospheric sooting flames using UV and visible excitation wavelengths.* Combustion and Flame, 2014. **161**(10): p. 2479–2491.

62. S.J. Harris, A.M. Weiner, and C. Cleveland Ashcraft, *Soot particle inception kinetics in a premixed ethylene flame.* Combustion and Flame, 1986. **64**(1): p. 65-81.

63. H. Chang and T.T. Charalampopoulos, *Determination of the wavelength dependence of refractive indices of flame soot.* Proceedings of the Royal Society of London: Series A, 1990. **430**: p. 577-591.

64. J. Reimann, S.A. Kuhlmann, and S. Will, *2D aggregate sizing by combining laser-induced incandescence (LII) and elastic light scattering (ELS).* Applied Physics B, 2009. **96**(4): p. 583-592.

65. H. Oltmann, J. Reimann, and S. Will, *Wide-angle light scattering (WALS) for soot aggregate characterization.* Combustion and Flame, 2010. **157**(3): p. 516-522.

66. D. Snelling, O. Link, K. Thomson, and G. Smallwood, *Measurement of soot morphology by integrated LII and elastic light scattering.* Applied Physics B, 2011. **104**(2): p. 385-397.

67. O. Link, D.R. Snelling, K.A. Thomson, and G.J. Smallwood, *Development of absolute intensity multi-angle light scattering for the determination of polydisperse soot aggregate properties.* Proceedings of the Combustion Institute, 2011. **33**: p. 847-854.

68. B.M. Crosland, K.A. Thomson, and M.R. Johnson, *Instantaneous in-flame measurement of soot volume fraction, primary particle diameter, and aggregate radius of gyration via auto-compensating laser-induced incandescence and two-angle elastic light scattering.* Applied Physics B, 2013. **112**(3): p. 381-393.

69. R.W. Weeks and W.W. Duley, *Aerosol-particle sizes from light emission during excitation by TEA CO.* Journal of Applied Physics, 1974. **45**(10): p. 4661-4662.

70. A.C. Eckbreth, *Effects of Laser-Modulated Particulate Incandescence on Raman Scattering Diagnostics.* Journal of Applied Physics, 1977. **48**: p. 4473-4479.

71. L.A. Melton, *Soot Diagnostics Based on Laser-Heating.* Applied Optics, 1984. **23**(13): p. 2201-2208.

72. D.R. Snelling, G.J. Smallwood, F. Liu, Ö.L. Gülder, and W.D. Bachalo, *A calibration-independent laser-induced incandescence technique for soot measurement by detecting absolute light intensity.* Applied Optics, 2005. **44**(31): p. 6773-6785.

73. J. Johnsson, H. Bladh, N.E. Olofsson, and P.E. Bengtsson, *Influence of soot aggregate structure on particle sizing using laser-induced incandescence: importance of bridging between primary particles.* Applied Physics B, 2013. **112**(3): p. 321-332.

74. F. Liu and G.J. Smallwood, *Study of Heat Conduction between Fractal Aggregates and the Surrounding Gas in the Transition Regime Using the DSMC Method*, in *40th Thermophysics Conference*. 2008: Seattle, Washington.

75. B.J. McCoy and C.Y. Cha, *Transport Phenomena in Rarefied-Gas Transition Regime.* Chemical Engineering Science, 1974. **29**(2): p. 381-388.

76. A.V. Filippov and D.E. Rosner, *Energy transfer between an aerosol particle and gas at high temperature ratios in the Knudsen transition regime.* International Journal of Heat and Mass Transfer, 2000. **43**(1): p. 127-138.

77. F. Liu, K.J. Daun, D.R. Snelling, and G.J. Smallwood, *Heat conduction from a spherical nano-particle: status of modeling heat conduction in laser-induced incandescence.* Applied Physics B, 2006. **83**(3): p. 355-382.

78. T. Lehre, B. Jungfleisch, R. Suntz, and H. Bockhorn, *Size distributions of nanoscaled particles and gas temperatures from time-resolved laser-induced-incandescence measurements.* Applied Optics, 2003. **42**(12): p. 2021-2030.

79. H.A. Michelsen, *Derivation of a temperature-dependent accommodation coefficient for use in modeling laser-induced incandescence of soot.* Applied Physics B, 2009. **94**(1): p. 103-117.

80. D.R. Snelling, F.S. Liu, G.J. Smallwood, and Ö.L. Gülder, *Determination of the soot absorption function and thermal accommodation coefficient using low-fluence LII in a laminar coflow ethylene diffusion flame.* Combustion and Flame, 2004. **136**(1-2): p. 180-190.

81. S. Maffi, S. De Iuliis, F. Cignoli, and G. Zizak, *Investigation on thermal accommodation coefficient and soot absorption function with two-color Tire-LII technique in rich premixed flames.* Applied Physics B, 2011. **104**(2): p. 357-366.

82. R. Starke, B. Kock, and P. Roth, *Nano-particle sizing by Laser-Induced-Incandescence (LII) in a shock wave reactor.* Shock Waves, 2003. **12**(5): p. 351-360.

83. H. Bladh, J. Johnsson, and P.-E. Bengtsson, *Influence of spatial laser energy distribution on evaluated soot particle sizes using two-colour laser-induced incandescence in a flat premixed ethylene/air flame.* Applied Physics B, 2009. **96**(4): p. 645-656.

84. F. Liu, M. Yang, F.A. Hill, D.R. Snelling, and G.J. Smallwood, *Influence of polydisperse distributions of both primary particle and aggregate size on soot temperature in low-fluence LII.* Applied Physics B, 2006. **83**(3): p. 383-395.

85. D.R. Snelling, F. Liu, G.J. Smallwood, and Ö.L. Gülder. *Evaluation of the Nanoscale Heat and Mass Transfer Model of the Laser-Induced Incandescence: Prediction of the Excitation Intensity*. in *Proc. 34th National Heat Transfer Conf.* 2000. Pittsburg, PA.

86. R.L. Vander Wal, T.M. Ticich, and A.B. Stephens, *Optical and Microscopy Investigations of Soot Structure Alterations by Laser-Induced Incandescence.* Applied Physics B, 1998. **67**: p. 115-123.

87. S. De Iuliis, F. Cignoli, S. Maffi, and G. Zizak, *Influence of the cumulative effects of multiple laser pulses on laser-induced incandescence signals from soot.* Applied Physics B, 2011. **104**(2): p. 321-330.

88. H. Bladh, J. Johnsson, and P.-E. Bengtsson, *On the dependence of the laser-induced incandescence (LII) signal on soot volume fraction for variations in particle size.* Applied Physics B, 2008. **90**(1): p. 109-125.

89. H. Bladh and P.-E. Bengtsson, *Characteristics of laser-induced incandescence from soot in studies of a time-dependent heat- and mass-transfer model.* Applied Physics B, 2004. **78**(2): p. 241-248.

90. H.A. Michelsen, P.O. Witze, D. Kayes, and S. Hochgreb, *Time-resolved laser-induced incandescence of soot: the influence of experimental factors and microphysical mechanisms.* Applied Optics, 2003. **42**(27): p. 5577-5590.

91. *Jing Ltd.* 2009 [cited October 13, 2014]; Available from: http://www.sootgenerator.com/.

92. *LIIscience*. [cited October 29, 2014]; Available from: liiscience.org.

93. L. Catalano. *Holthuis and Associates*. [cited October 13, 2014]; Available from: www.flatflame.com.

94. F. Migliorini, S. De Iuliis, F. Cignoli, and G. Zizak, *How "flat" is the rich premixed flame produced by your McKenna burner?* Combustion and Flame, 2008. **153**(3): p. 384-393.

95. D.R. Snelling, K.A. Thomson, G.J. Smallwood, and Ö.L. Gülder, *Two-dimensional imaging of soot volume fraction in laminar diffusion flames.* Applied Optics, 1999. **38**(12): p. 2478-2485.

96. Ö.L. Gülder, D.R. Snelling, and R.A. Sawchuk, *Influence of hydrogen addition to fuel on temperature field and soot formation in diffusion flames.* Symposium (International) on Combustion, 1996. **26**(2): p. 2351-2358.

97. M. Charwath, R. Suntz, and H. Bockhorn, *Constraints of two-colour TiRe-LII at elevated pressures.* Applied Physics B, 2011. **104**(2): p. 427-438.

98. M.A. Dansson, M. Boisselle, M.A. Linne, and H.A. Michelsen, *Complications to optical measurements using a laser with an unstable resonator: a case study on laser-induced incandescence of soot.* Applied Optics, 2007. **46**(33): p. 8095-8103.

99. H. Oltmann, J. Reimann, and S. Will, *Single-shot measurement of soot aggregate sizes by wide-angle light scattering (WALS).* Applied Physics B, 2012. **106**(1): p. 171-83.

100. A.G. Gaydon, *The Spectroscopy of Flames*. 2nd ed. 1974, London: Chapman and Hall. 412.

101. A.C. Eckbreth, *Laser diagnostics for combustion temperature and species*. 2nd ed. Combustion science and technology book series, 3. 1996, Amsterdam: Gordon & Breach. 596.

102. S. Roy, J.R. Gord, and A.K. Patnaik, *Recent advances in coherent anti-Stokes Raman scattering spectroscopy: Fundamental developments and applications in reacting flows.* Progress in Energy and Combustion Science, 2010. **36**: p. 280-306.

103. F. Vestin, M. Afzelius, C. Brackmann, and P.E. Bengtsson, *Dual-broadband rotational CARS thermometry in the product gas of hydrocarbon flames.* Proceedings of the Combustion Institute, 2005. **30**: p. 1673-1680.

104. X. López-Yglesias, P.E. Schrader, and H.A. Michelsen, *Soot maturity and absorption cross sections.* Journal of Aerosol Science, 2014. **75**(0): p. 43-64.

105. A.R. Coderre, K.A. Thomson, D.R. Snelling, and M.R. Johnson, *Spectrally resolved light absorption properties of cooled soot from a methane flame.* Applied Physics B, 2011. **104**(1): p. 175-188.

106. R.L. Vander Wal and M.Y. Choi, *Pulsed laser heating of soot: Morphological changes.* Carbon, 1999. **37**: p. 231-239.

107. R.L. Vander Wal, M.Y. Choi, and K.O. Lee, *The Effects of Rapid Heating of Soot - Implications When Using Laser-Induced Incandescence for Soot Diagnostics.* Combustion and Flame, 1995. **102**(1-2): p. 200-204.

108. H.A. Michelsen, P.E. Schrader, and F. Goulay, *Wavelength and temperature dependences of the absorption and scattering cross sections of soot.* Carbon, 2010. **48**(8): p. 2175-2191.

109. F. Goulay, P.E. Schrader, and H.A. Michelsen, *Effect of the wavelength dependence of the emissivity on inferred soot temperatures measured by spectrally resolved laser-induced incandescence.* Applied Physics B, 2010. **100**(Copyright 2011, The Institution of Engineering and Technology): p. 655-63.

110. G. Cléon, T. Amodeo, A. Faccinetto, and P. Desgroux, *Laser induced incandescence determination of the ratio of the soot absorption functions at 532 nm and 1064 nm in the nucleation zone of a low pressure premixed sooting flame.* Applied Physics B, 2011. **104**(2): p. 297-305.

111. F.S. Liu, B.J. Stagg, D.R. Snelling, and G.J. Smallwood, *Effects of primary soot particle size distribution on the temperature of soot particles heated by a nanosecond pulsed laser in an atmospheric laminar diffusion flame.* International Journal of Heat and Mass Transfer, 2006. **49**(3-4): p. 777-788.

112. A.V. Filippov, M. Zurita, and D.E. Rosner, *Fractal-like aggregates: Relation between morphology and physical properties.* Journal of Colloid and Interface Science, 2000. **229**(1): p. 261-273.

113. *CAST, Combustion Aerosol Standard.* 2009 [cited November 6, 2014]; Available from: http://www.sootgenerator.com/.

114. A. Malik, H. Abdulhamid, J. Pagels, J. Rissler, M. Lindskog, P. Nilsson, R. Bjorklund, P. Jozsa, J. Visser, A. Spetz, and M. Sanati, *A potential soot mass determination method from resistivity measurement of thermophoretically deposited soot.* Aerosol Science and Technology, 2011. **45**: p. 284-294.

115. A.C. Eckbreth, *Experimental Diagnostics in Gas Phase Combustion Systems*, in *Progress in Astronautics and Aeronautics 53*, B.T. Zinn, Editor. 1977, AIAA: New York. p. 517-547.

116. D. Snelling, K. Thomson, F. Liu, and G. Smallwood, *Comparison of LII derived soot temperature measurements with LII model predictions for soot in a laminar diffusion flame.* Applied Physics B, 2009. **96**(4): p. 657-669.

117. M.H. de Andrade Oliveira, C.C.M. Luijten, and L.P.H. de Goey. *Soot measurements in laminar flames of gaseous and (prevaporized) liquid fuels*. in *4th European combustion meeting*. 2009. Vienna, Austria.

118. E. Robert and P.A. Monkewitz, *Experimental realization and characterization of unstretched planar one-dimensional diffusion flames.* Combustion and Flame, 2013. **160**(3): p. 546-556.

119. H.A. Michelsen, F. Liu, B.F. Kock, H. Bladh, A. Boiarciuc, M. Charwath, T. Dreier, R. Hadef, M. Hofmann, J. Reimann, S. Will, P.-E. Bengtsson, H. Bockhorn, F. Foucher, K.P. Geigle, C. Mounaïm-Rousselle, C. Schulz, R. Stirn, B. Tribalet, and R. Suntz,

Modeling Laser-Induced Incandescence of Soot: A summary and comparison of LII models. Applied Physics B, 2007. **87**: p. 503–521.

9 Contribution to papers

I.   H. Bladh, J. Johnsson, **N.-E. Olofsson**, A. Bohlin, and P.-E. Bengtsson,
      Optical soot characterization using two-color laser-induced incandescence (2C-
      LII) in the soot growth region of a premixed flat flame. Proceedings of the
      Combustion Institute, 2011. 33: p. 641-648.
      I set up the experiment and conducted the measurements together with Henrik
      Bladh. I took also part in writing of the manuscript and participated in discussions
      about the results their implications.

II.   H. Bladh, J. Johnsson, J. Rissler, H. Abdulhamid, **N.-E. Olofsson**, M. Sanati,
      J. Pagels, and P.-E. Bengtsson, Influence of soot particle aggregation on time-
      resolved laser-induced incandescence signals. Applied Physics B, 2011. 104(2):
      p. 331-341.
      I participated in the writing process of the manuscript and discussions about the
      results and their implications.

III. **N.-E. Olofsson**, H. Bladh, A. Bohlin, J. Johnsson, and P.-E. Bengtsson, Are
      Sooting Premixed Porous-Plug Burner Flames One-Dimensional? A Laser-
      Based Experimental Investigation. Combustion Science and Technology,
      2013. 185(2): p. 293-309.
      I was the main responsible for the experimental work, evaluation of the results and
      writing of the manuscript.

IV.   M.H. de Andrade Oliveira, **N.-E. Olofsson**, J. Johnsson, H. Bladh, A. Lantz,
      B. Li, Z.S. Li, M. Aldén, P.-E. Bengtsson, C.C.M. Luijten, and L.P.H. de
      Goey, Soot, PAH and OH measurements in vaporized liquid fuel flames. Fuel,
      2013. 112(0): p. 145-152.
      I conducted the LII measurements together with Henrik Bladh and took part in the
      discussions about the results of the LII measurements and their implications.

V.   **N.-E. Olofsson**, J. Johnsson, H. Bladh, and P.-E. Bengtsson, Soot sublimation
      studies in a premixed flat flame using laser-induced incandescence (LII) and
      elastic light scattering (ELS). Applied Physics B, 2013. 112(3): p. 333-342.
      I was the main responsible for the experimental work, evaluation of the results and
      writing of the manuscript.

VI.   H. Bladh, **N.-E. Olofsson**, T. Mouton, J. Simonsson, X. Mercier, A. Faccinetto, P.-E. Bengtsson, and P. Desgroux, Probing the smallest soot particles in low-sooting premixed flames using laser-induced incandescence. Proceedings of the Combustion Institute, 2014. 35

I was the main responsible for the experimental work conducted in Lund and took part in writing the manuscript, where I wrote the experimental part and participated in the discussions about the results and their implications.

VII.   E. Nordström, **N.-E. Olofsson**, J. Simonsson, J. Johnsson, H. Bladh, and P.-E. Bengtsson, Local gas heating in sooting flames by heat transfer from laser-heated particles investigated using rotational CARS and LII. Proceedings of the Combustion Institute, 2014. 35

Together with Emil Nordström I was the main responsible for the experimental work, where I took care of the LII part and he cared for the CARS measurements. I was also responsible for the LII related part of the manuscript and participated in the discussions about the results and their implications.

VIII.   E. Robert, **N.-E. Olofsson**, H. Bladh, J. Johnsson, and P.-E. Bengtsson, Soot formation in unstrained diffusion flames. Combustion Science and Technology, 2014, DOI: 10.1080/00102202.2014.958219

I was responsible for the LII measurements, wrote the experimental part related to LII in the manuscript and participated in discussions about the results and their implications.

IX.   **N.-E. Olofsson**, J. Simonsson, S. Török, H. Bladh, and P.-E. Bengtsson, Evolution of properties for aging soot in premixed flat flames studied by laser-induced incandescence and elastic light scattering. Submitted to Applied Physics B, 2014.

I was the main responsible for the experimental work, evaluation of the results and writing of the manuscript.

X.   J. Simonsson, **N.-E. Olofsson**, S. Török, P.-E. Bengtsson, and H. Bladh, Wavelength dependence of extinction in sooting flat premixed flames in the visible and near infrared regimes. Submitted to Applied Physics B, 2014.

I assisted Johan Simonsson in the experimental work and I participated in the writing process of the manuscript and the discussions about the results and their implications.